Particle Physics at the University of Pittsburgh

Summary Report for Proposal Period FY'09–11

Joe Boudreau, Steven Dytman, James Mueller, Donna Naples,

Vittorio Paolone, Vladimir Savinov, and Paul Shepard

October 1, 2012

Contents

TASK B: FERMILAB CDFII PROGRAM

1 Program Outline

This report constitutes the final report for the CDF task B program at Fermilab for the University of Pittsburgh which ended in May, 2012. Additional work is continuing under a new DOE grant. The group from the University of Pittsburgh working on CDF has consisted of Joseph Boudreau, Paul Shepard, and Hao Song.

Joe Boudreau has concluded his work on CDF on CP violation in the B_s system, and on a number of precision measurements of B lifetimes, with three publications, Ref [1], [2] on CP violation, and [3] on precision lifetime measurements. Both Paul Shepard and Hao Song are continuing to work on the B_c meson.

Over the past year Hao Song, a graduate student, has been working with Paul Shepard and Fermilab collaborators to produce a measurement of the B_c lifetime in the exclusive channel $B_c^+ \to J/\psi\pi^+$. This work is has been completed. Hao has both produced a draft of his thesis and the CDF Collaboration is reviewing a Physical Review Rapid Report which Hao and Shepard have prepared. Hao expects to defend his thesis by November, 2012. Since Paul Shepard retired in January, 2012, he has been supervising Hao's work as a Professor Emeritus.

In addition Turgun Nigmanov has been working with Paul Shepard to update the B_c semileptonic dataset to approximately 8 fb^{-1}. In this case the plan is to update previous measurements of both the B_c lifetime and relative cross section using the full CDF dataset. These activities are discussed more fully below.

2 B_c Studies in Run II

2.1 Measurement of the B_c Lifetime in the Exclusive Channel $B_c^+ \to J/\psi\pi^+$

The collaboration between Paul Shepard and Hao Song at the University of Pittsburgh and Jeff Apple, Pat Lukens, Ron Moore, and William Wester at Fermilab has completed the made measurement of the B_c lifetime in the exclusive channel $B_c^\pm \to J/\psi\pi^\pm$ using the currently available CDF dataset. With the help of our Fermilab collaborators we have prepared a draft Physical Review D Rapid Report which is in the final review process within the CDF Collaboration. Hao Song has also produced a draft of his Ph.D. thesis on this measurement which he is currently revising and he expects to defend his thesis by November, 2012.

A preliminary result can be found at the following `http://www-cdf.fnal.gov/physics/new/bottom/110804.blessed-bc-lifetime/welcome.html`. The final result has not changed and we will report for the average lifetime of the B_c meson in the decay channel $B_c^\pm \to J/\psi\pi^\pm$ the result: $\tau = 0.452 \pm 0.048(stat) \pm 0.027(syst)$ ps. Here we show only an invariant mass distribution and a proper decay length $c\tau$ distribution of the $B_c^+ \to J/\psi\pi^+$ signal candidates.

The reconstructed mass distribution for the B_c^+ candidates is shown in Fig. 1. The signal region lies between two background sideband regions and has 1496 B_c^+ candidates. The two sideband regions consist of a lower sideband from 6.16 to 6.21 GeV/c^2 and an upper sideband from 6.33 to 6.60 GeV/c^2, as shown in the hatched areas. The lower sideband is narrow to avoid contamination from semileptonic B_c^+ decays where the lepton is misidentified as a pion.

Figure 2 shows the $c\tau$ distribution of the $J/\psi\pi$ signal events. The fit projections are overlaid.

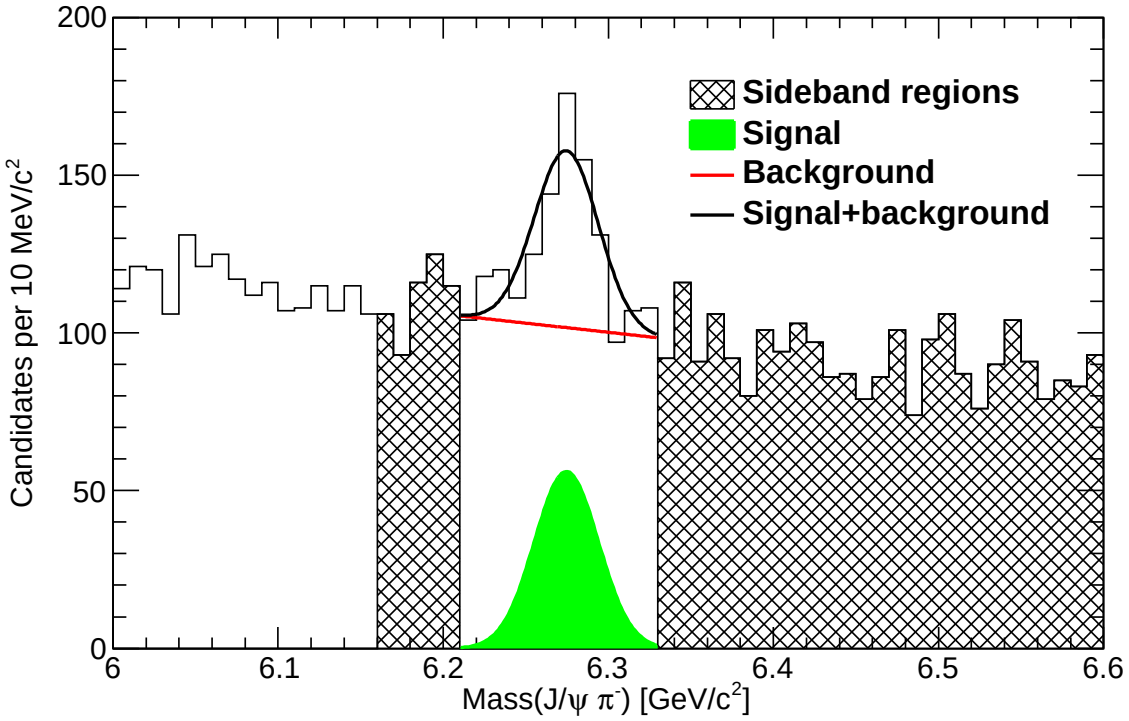

Figure 1: Invariant-mass distribution of $J/\psi\pi$ candidates. The hatched areas are the sideband regions and the signal region lies between them. The fit result is overlaid in the signal region, as well as the signal and background components.

2.2 B_c Semileptonic Decays

Paul Shepard and Turgun Nigmanov have extended the anaylsis of the B_c semileptonic decays in both the muon and electron channels to include the entire run II CDF dataset of approximately 8 fb^{-1} of integrated luminosity. Much of the work on the various backgrounds is complete and we have a preliminary result for the measurement of the relative cross section times branching fraction $\frac{\sigma(B_c)*\mathcal{B}(B_c\to J/\psi\mu^+\nu)}{\sigma(B^+)*\mathcal{B}(B^+\to J/\psi K^+)}$ in $p\bar{p}$ collisions at $\sqrt{s} = 1.96$ TeV in the muon channel. The statistical uncertainty in the new result is 0.013 compared with a statistical uncertainty of 0.040 in our previous result based on a sample with 1 fb^{-1}. The evaluation of the systematic errors is work in progress, but we expect to present our new results to the B group at CDF soon.

3 b-hadron Lifetimes and CP violation

Joe Boudreau and a number of former students and postdocs have conducted studies of b-hadron lifetimes and CP violation in the B_s^0 sector at CDF. Boudreau is not requesting any further funding activities related to the CDF experiment; however here we report progress in lifetime measurement and describe our efforts to reach a conclusion on the measurement of the CP-violating phase, β_s. Precise measurements of b-hadron lifetimes and of the CP violating phase both have strong physics

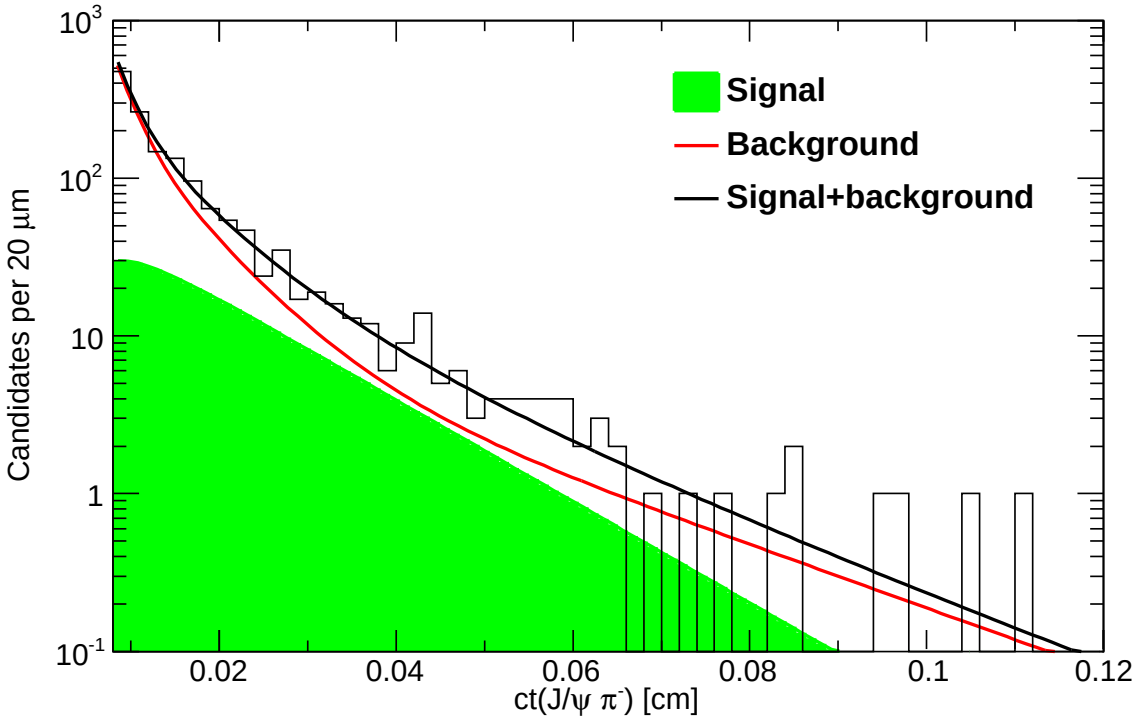

Figure 2: Decay-length distribution of $J/\psi\pi$ candidates. The total fit projection, along with individual contributions from signal and backgroud, is overlaid.

motivations as we will describe below. To assist in the update and publication of these established analyses we have supported for short periods of time two experienced CDF Ph.D's, both of them holding degrees from the University of Oxford. We supported Sneha Malde between March and August of 2009 to update the analysis of the B^+, B^0, and Λ_b lifetimes. In addition, we supported Louise Oakes in August and September to help bring the β_s analysis to publication, following the approval in May 2010.

The CP-violating phase β_s is a CP-violation parameter (like the well known angle β measured at the B-factories) which is cleanly accessible to experimental measurement through the measurement of time-dependent, angle-dependent differential rates in the flavor-tagged decay $B_s^0 \to J/\psi\phi$. The value of this phase is close to zero: $\beta_s = (1.9 \pm 0.1) \cdot 10^{-2}$, which indicates that appreciable CP violation should not occur in the decay. If significant CP violation were found to occur, it would be a sign of new physics, such as supersymmetric particles or a fourth generation.

Precise measurements of b-hadron lifetimes and their ratios have been important as a check of the theoretical approach known observables in heavy quark hadrons known as the Heavy Quark Expansion (HQE). The HQE is used as a tool to calculate many flavor observables, such as Γ_{12}^s, which enters the decay width difference in the B_s^0 system as well as several CP violation effects. Lifetime measurements became particularly relevant again Last year, when D0 caused excitement by releasing a measurement of an anomalously large muon semileptonic asymmetry from B decays. Several

theorists called for more precise measurements of b-hadron lifetimes. Precision measurements of these lifetimes not only are a control of the HQE, but are also sensitive to new particles and interactions needed for a full explanation of the D0 result.

3.1 b Hadron Lifetimes in Final States containing a J/ψ

Measurement of b-hadron lifetimes and lifetime ratios in the fully reconstructed decay modes $B^+ \to J/\psi K^+$, $B^0 \to J/\psi K^{0*}$, $B^0 \to J/\psi K^0_s$,and $\lambda^0_B \to J/\psi \Lambda^0$ using 4.3 fb^{-1} of data were published[3]. The published lifetimes for $B+$, B^0, and Λ_b, as well as the lifetime ratios $\tau(B^+)/\tau(B^0)$ and $\tau(\Lambda^0_b)/\tau(B^0$ are all presently world-leading. Boudreau and Malde, together with our parter Juan Pablo Fernandez from CIEMAT, Madrid, were the principal authors of this analysis. Some comparison plots are shown in Fig. 3. The two most recent independnent measurements of $\tau(\Lambda^0_b)$ from CDF together indicate a higher value than that indicated by the long and sometimes controversial history of previous measurement.

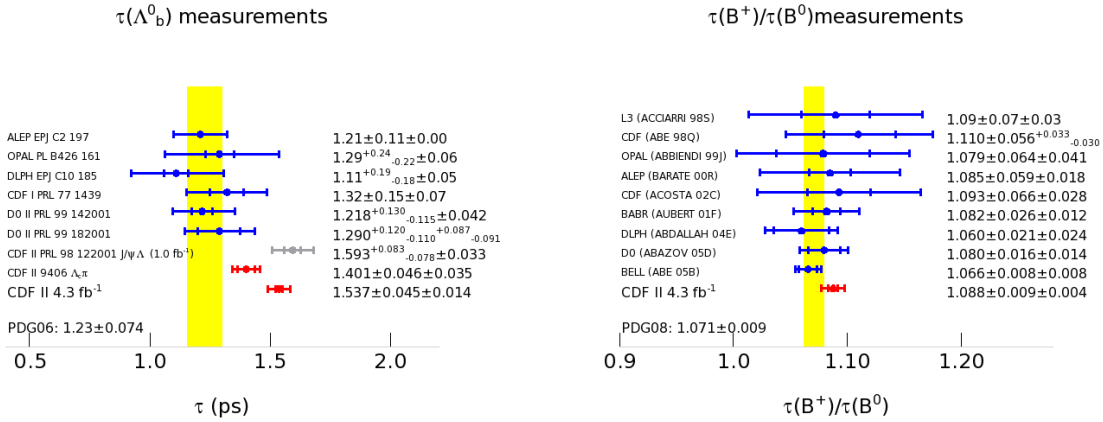

Figure 3: Comparison of recent CDF b hadron lifetime measurements with the world average values, and with previous measurement. Right: the Λ_b lifetime; our measurement is labeled CDFII 4.3 pb^{-1}; an independent measurement using a different decay is shown above our measurement, in red, and the grayed-out point is our previous published measurement which is now superseded. World average values do not include the points shown in red or gray. Left: τ_+/τ_0.

3.2 CP Violation in the decay $B^0 \to J/\psi\phi$

The University of Pittsburgh has been deeply involved in the analysis of the CP-violating phase since the first measurements were carried out in 2007. The core of the complicated fitter was written by Boudreau; his graduate student Chunlei Liu added several features like background and variable dilutions, and former Pitt postdoc Karen Gibson worked out many inputs to the fitter (like background angular distributions) and organized the whole effort for many years. We also worked out a complicated normalization for the likelihood, extended it to include an S-wave contribution (by doing the necessary phenomenology in addition to implementing it in code). Much of this is described in a paper submitted in October 2010 to JHEP[2], which was written by Boudreau the principal authors of the β_s analysis.

During the last years of our involvement we were also active in combining of CDF's β_s result with theoretical expectations on the strong phases and the effect of CP violation on the width difference $\Delta\Gamma$. This is illustrated in Figs. 4 and 5. These series of plots show the likelihood function

integrated via Markov Chain Monte Carlo, a procedure which we developed here. Markov chains from the procedure can be projected onto the space of physically interesting variables, and extra constraints and conditions added without large amounts of additional computation. For generic short-distance weak interactions, theory predicts a mixing of the two mass eigenstates which erases the width difference $\Delta\Gamma_s$ as CP violation increases, according to $\Delta\Gamma_s = 2 \cdot |\Gamma_{12}^s| \cos(2beta_s)$. This is called mixing-induced CP violation (MICP violation). The theoretical constraints arising from MICP violation are codisplayed with our likelihood in Fig. 4, left, and the projection of the likelihood into β_s space is shown in the middle. On the right in Fig. 4, we show the likelihood again, after imposing the constraint of MICP violation.

Fig. 5 contains plots of the probability density in the space of the strong phases and β_s, and is intended to show the way in which these two variables are correlated, through conditional probabilities. By boxing one of the major modes of probability density on the left (top row of Fig. 5), one loses one of the β_s solutions on the right. Conversely, by boxing off one of the β_s solutions, one loses one of the solutions in the strong phases (bottom row of Fig. 5). This is relevant because of a theoretical prediction[8] for the strong phases, shown as the green dot in this series of plots. Using the green dot to tag the correct mode of probability, from the top left plot in Fig. 5 one obtains $\beta_s \in [0.09, 0.32]$, corresponding to a value of $\beta_s = (11.7 \pm 6.6)^\circ$.

We have now finalized a comprehensive paper containing these and other CDF results on the β_s analysis which includes CP violation parameters but also all of the parameters that can be extracted in the decay, including decay amplitudes, phases, the S-wave contribution, and the B_s lifetime[1]. An additional paper based on the full CDF dataset, based on the same analysis code developed by us, has been published after Boudreau's departure from CDF[7].

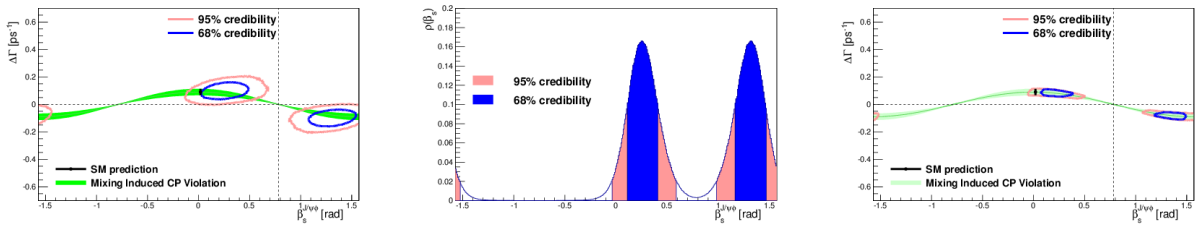

Figure 4: The likelihood function in integrated and projected onto physically interesting parameters spaces. From left to right: the probability density in β_s, $\Delta\Gamma^s$ space, shown together with the expectation from Mixing Induced CP violation (the band); a projection onto β_s space alone; and the 2D contour constrained by the assumption of mixing-induced CP violation (MICP).

4 Conferences

Includes only conferences not previously reported.

1. Hao Song, "Measurement of the lifetime of the B_c meson using fully reconstructed $B_c \to J/\psi\pi$ decays at CDF," presented at the APS meeting in Anaheim, CA, May 3, 2011

2. Hao Song, "B_c lifetime measurement in fully reconstructed channel $B_c \to J/\psi\pi$ at CDF," presented at the Workshop on Heavy Quarkonium, Damstadt, Germany, October 4-7, 2011.

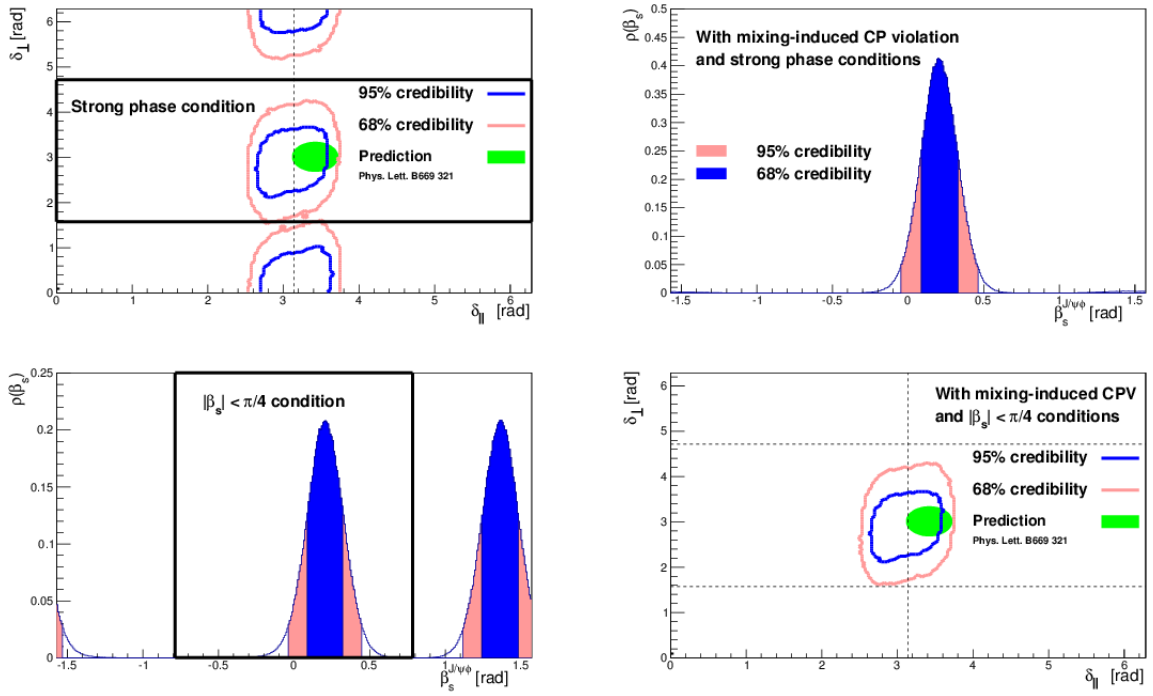

Figure 5: Conditional probability densities illustrate the correlations between strong phases and the CP violation parameters in the full multidimensional parameter space. Top row: left, a plot of the strong phases shown together with a theoretical prediction from [8] and a black box indicating a region to be masked off; right, the probability density in β_s subject to the condition that the strong phases lie within the box. In the bottom row we illustrate the correlation differently, by boxing the probability density in β_s by requiring that it lie in the box, on the left, and show on the right the effect upon the probability density in the space of the strong phases. Plots on the right are therefore identified with the solution predicted in Ref. [8].

References

[1] T. Aaltonen *et al.,* (CDF Collaboration), "Measurement of the CP-violating phase β_s in $B_s^0 \to J/\psi\phi'$ decays with the CDFII Detector " Phys. Rev. D **85**, 072002 (2012).

[2] F. Azfar *et al.,*, "Formulae for the analysis of the flavor-tagged decay $B_s^0 \to J/\psi\phi'$," JHEP vol. 2010 no. 11, 158 (2010)

[3] T. Aaltonen *et al.,* (CDF Collaboration), "Measurement of b Hadron Lifetimes in Exclusive Decays Containing a J/ψ in $p\bar{p}$ Collisions at $\sqrt{s} = 1.96$ TeV," Phys. Rev. Lett. **106**, 121804 (2011).

[4] "Measurement of the $B_c^{\pm}$ Meson Lifetime Using $B_c^{\pm} \to J/\psi + l + X$ Decays," University of Pittsburgh thesis, Nov., 2008, 301pp, FERMILAB-THESIS-2008-82.

[5] http://www-cdf.fnal.gov/physics/new/bottom/080327.blessed-BC_LT_SemiLeptonic/blessed-bc-lifetime.pdf

[6] http://www-cdf.fnal.gov/physics/new/bottom/090305.blessed-bc-slXsec/bcXsect_public.pdf

[7] T. Aaltonen *et al.,* (CDF Collaboration), "Measurement of the Bottom-Strange Meson Mixing Phase in the Full CDF Data Set" arXiv:1208.2967

[8] M. Gronau and J. Rosner, Phys. Lett. B **669**, 321 (2008)

TASK D: NEUTRINO PHYSICS

Task D supports Pitt's neutrino group which includes PIs Dytman, Naples and Paolone. The present group also includes postdoctoral research associate Danko, and thesis students Isvan (MINOS), Eberly (MINERνA), Ren (MINERνA) and Hansen (T2K). Neutrino oscillation phenomona is well established and the field has entered into a period of precision measurements and a detailed understanding of the neutrino mixing matrix. This report summarizes our progress on ongoing experiments which are designed to make significant contributions to this effort: MINOS, MINERνA T2K and the future planned very long-baseline experiment LBNE. An overview of PIs' efforts on each experiment is given below.

5 MINOS

The MINOS effort at Pittsburgh currently includes faculty members D. Naples and graduate student Zeynep Isvan. The MINOS long-baseline neutrino oscillation experiment, which combines Fermilab's high-rate NuMI beam with a 735 km neutrino path-length, was designed to explore the region of the atmospheric neutrino oscillation signal. Among the physics results that MINOS has produced is the most precise determination to date of the neutrino squared mass difference, $\Delta m^2_{23} = (2.32^{+0.12}_{-0.08}) \times 10^{-3}$ eV^2 and a constraint on the mixing, $\sin^2(2\theta) > 0.90$ (90% C.L.) [1]. Other important physics topics that can be addressed by MINOS include searching for electron neutrino appearance to constrain the unknown mixing parameter, θ_{13} [2] and providing the first direct constraint on antineutrino oscillation parameters using a tagged event sample [3].

Overview of University of Pittsburgh's Activities: Pittsburgh has had a long history of involvement on MINOS starting in 1998 when Naples and Paolone joined the experiment. The group has make important contributions to many aspects of the experiment. These include early design work on alternative far detector technologies, design of the beamline muon monitoring system, near detector assembly and installation, calibration detector and calibration analysis work. Analysis contributions include measurement of charged-current total cross section [4] (Pitt Thesis Bhattacharya 2009) and more recently antineutrino oscillation [3] & [5] and non-standard interaction analyses (Pitt Thesis Isvan 2011).

The current active members of the Pitt MINOS group are Naples and Graduate student Isvan. The main activity of the group has been analysis of antineutrino oscillation samples. Naples is currently co-convenor of the Disappearance Working Group and was one of the original convenors of the Antineutrino Oscillation Group. Postdoc Danko made important past contributions to analysis of the first antineutrino data sample obtained in the NuMI nominal running mode. Thesis student Z. Isvan, whose thesis further constrains antineutrino oscillation parameters and combines neutrino and antineutrino data samples to constrain new physics, has also been a key contributor to past and ongoing antineutrino analyses.

6 Minerva

The Minerva group at Pittsburgh includes faculty members S. Dytman, D. Naples and V. Paolone, and graduate students B. Eberly and L. Ren. MINERνA is designed for precision measurements of the neutrino cross section processes whose uncertainties are among the largest contributions to the overall error budget for next-generation neutrino oscillation experiments. The first physics results will focus on QE reactions in scintillator and inclusive muon response from solid targets. Early results have been presented at recent conferences [6].

The MINERνA detector is located directly in front of the MINOS near detector ∼100m underground on the Fermilab site and has been in data-taking mode since 2009. The detector is composed of modules which are hexagons about 2.4 m on a side. The modules are pure scintillator in the central region with a fiducial volume of about 6.8 tons. The stack also contains solid targets of carbon, iron, water, and lead with a liquid helium vessel directly in front of the main stack. The completed full detector has about 127 scintillator planes, each 1.7 cm thick. Each plane has about 125 triangular bars. Surrounding this inner region is mixed metal/scintillator regions for containment. Although this arrangement is optimized for charged particle identification, neutral particles are also easily seen. The MINOS magnetized detector is used for momentum measurement and charge ID. Runs as end of October, 2011 have accumulated 1.75×10^{20} POT for ν_μ and about 1.73×10^{20} POT for $\overline{\nu}_\mu$, all with the full detector and all in the NUMI LE configuration where the flux peaks at about 3 GeV. We estimate a total of 1.36 million CC events for a 6.43 ton fiducial mass (scintillator only) and $4x10^{20}$ POT (our allotment in ν_μ mode). At the same time, about 220,000 events will come from separate iron and lead targets.

Progress of University of Pittsburgh's Activities: Pittsburgh was a charter member of MINERνA and has made significant contributions in recent years.

Paolone was the project manager (Level 2) for the Electronics and DAQ, working closely with Paul Rubinov, a Fermilab electronics designer and scientist. This work involved, in addition to the procurement of several hundred front-end readout boards (FEB), the design and development of a test-stand to test and calibrate these boards. He has involved several undergraduates in the operation of the test-stand. Currently, Paolone co-leads the EM working group and is chairman of the speakers committee. Work in the EM group involved building algorithms to identify gammas and electron showers over a wide range in energy with both high efficiency and purity. In addition algorithms needed to reconstruct both shower direction and energy have been developed by the students. Graduate students Jaewon Park (University of Rochester) and Jose Palomino (Centro Brasileiro de Pesquisas Fsicas, Rio de Janeiro, Brazil/University of Pittsburgh) make regular updates on their progress to the weekly EM working group meetings. Park is studying neutrino-electron scattering and electron neutrino CCQE cross-sections while Palomino is studying resonance CC π^0 production cross-section and have been, under EM working group supervision, made steady progress. The speakers committee is responsible for determining priority conferences, speakers, and reviewing conference presentations.

Dytman is co-leader of the exclusive final states working group and of the Pion Production working group. Naples has stepped up her effort on Minerva this past year and now leads the Calibrations working group, replacing Dytman. Graduate student B. Eberly (Dytman) has been on MINERνA for over 4 years and has made major reconstruction and calibration contributions to the experiment. L. Ren (Naples) joined this year and is contributing to the flux and inclusive working groups. Details are provided in the subsections that follow.

7 T2K

The T2K effort at Pittsburgh includes faculty members S. Dytman, D. Naples and V. Paolone, postdoc I. Danko, and graduate student D. Hansen. The T2K (Tokai to Kamioka) experiment in Japan is part of the next generation exploration of neutrino mixing phenomena. In the current picture of three generation neutrino oscillations, two of the three mixing angles, $\theta_{12}(\sim 34^\circ)$ and $\theta_{23}(\sim 45^\circ)$, and two independent mass differences, $\Delta m^2_{23}(\approx 2.3\times10^{-3}eV^2)$ and $\Delta m^2_{12}(\approx 8\times10^{-5}eV^2)$, have been measured. The current generation of reactor and accelerator off-axis long-baseline oscillation experiments will measure the remaining unknown mixing angle, θ_{13}, the ordering of the neutrino

mass states (whether $\Delta m^2_{13} > 0$ or < 0). If θ_{13} is not vanishingly small, the possibility of a non-zero CP violating phase, δ, in the neutrino sector will also be explored at future long baseline experiments.

T2K uses the J-PARC facility operating in Tokai Japan. The beam is aimed to illuminate the off-axis detectors at an angle of 2.5° off the beam axis. The resulting peaked beam spectrum will allow the ν_e beam and NC feed-down background from high energy neutrinos to be much reduced. The existing SuperKamiokande 50 kton water Cerenkov situated 295 km away is used to detect the oscillated neutrinos. The ND280 site, 280m from the beam source, houses a suite of detectors needed to measure the beam flux and ν_e appearance backgrounds. ND280 consists of an on-axis detector(INGRID) and a set of off-axis detectors (P0D, FGD, TPC, ECAL and SMRD). The primary purpose the INGRID is to measure and monitor the beam profile and stability using neutrino interactions. Our main effort is with the off-axis sub-detector "Pi-Zero Detector" (P0D) is of interest. It is optimized to measure the neutral current π^o production ν_e appearance background in water but also will include measurments of the intrinsic ν_e beam content. We are also starting to contribute to a pion production measurement in the FGD. For a detailed description of the experiment please see [7].

Both the Near Detector (ND280) and accelerator are complete and had been taking neutrino data since January 2010 until the Japan earthquake of March 11, 2011 shutdown experimental operations for the near future. The accelerator had been running just below the scheduled design intensity for JFY 2010 of 200 kW, at 145 kW and T2K had accumulated 14.5×10^{19} POT just prior to the earthquake.

The primary goal of T2K was to improve sensitivity to θ_{13} by about an order of magnitude over, as of last year, the current best limit from the CHOOZ experiment. In addition, T2K can also improve substantially on oscillation parameters in the $2 \rightarrow 3$ sector. T2K already has a preliminary result for θ_{13} based on 14.5×10^{19} POT. The result, based on an observed six fiducial single-ring e-like events with a prediced background of 1.5 ± 0.3 assuming no oscillations, excludes $\sin^2(2\theta_{13}) = 0$ at the 2.5σ level [8].

Progress of University of Pittsburgh's Activities: T2K presently has a significant and important data sample on hand and again has an operating and functional detector/accelerator in the near future. The group had made major past hardware contributions including responsibility for P0D electronics testing, installation and operation (Naples, Paolone, and Danko). Dytman also made contributions to Light Injection control electronics and DAQ for the P0D.

Paolone had ongoing roles in P0D post-earthquake recovery and Danko is a co-convenor of the calibration working group. Paolone along with graduate student Hanson have developed the software to identify and flag stopping muons in the POD and measure their charge and momenta. This work was exploited to study ν_μ CC interactions that are fully contained within the POD. Paolone is the IB representative of the Pittsburgh group on T2K, the chairman of the T2K safety committee and was the OnSite Supervisor(OSS) during the Fall of 2011. During the repair phase groups wishing to perform work in the experimental hall needed to submit a risk assessment and method statement to the safety committee for approval prior to start of work to ensure proper safety procedures are followed. Paolone along with Alysia Marino (University of Colorado), were co-editors of the P0D NIM paper which was published in early 2012.

8 LBNE

The LBNE effort at Pittsburgh includes faculty members D. Naples and V. Paolone, and a postdoc(s) yet to be determined (funds are requested in this proposal). The next level in neutrino oscillation experiments sensitivity will be probed by the LBNE (Long-Baseline Neutrino Experiment) which

is currently in the planning phase. LBNE will use a high intensity "super-beam" (0.7-2.3MW) produced at Fermilab and a massive detector in the DUSEL underground lab in the Homestake mine in South Dakota about 1300 km from the source. This unprecedented long-baseline will allow sensitivity to oscillation parameters that may be outside the reach of the current generation of experiments, such as, the size of the CP violating phase, δ_{CP} which governs CP violation in the neutrino sector, and the sign of the mass difference, Δm^2_{13}, which enters into to the appearance probability though matter effects.

Progress of University of Pittsburgh's Activities: The main focus of the Pitt group had been design work on the Near Detector suite that would determine the beam fluxes, flavor composition and neutrino induced backgrounds with high precision. The experiment is in the planning phase with the design of the far detector and beamline soon to solidify. Naples as Paolone ramped up work on defining the Near Detector requirements and finalizing its design. Paolone had been appointed level 4 manager of the scintillator-based tracking detector option. This task included costing estimates for this near detector option. Included in these estimates were the disassembly and re-assembly of the MINERνA detector into the LBNE near detector hall, replacement of the photo-sensors from PMT's to MPPC's, and integration of the T2K/ND280 water target design. Paolone had specifically performed a costing estimate based on the water target design used in the T2K FGD Detector.

References

[1] "Measurement of the neutrino mass splitting and flavor mixing by MINOS.", by MINOS Collaboration, (P. Adamson *et al.*), Phys. Rev. Lett. 106, 181801 (2011).

[2] "Improved search for muon-neutrino to electron-neutrino oscillations in MINOS.", by MINOS collaboration (P. Adamson *et al.*), Phys. Rev. Lett. 107, 181802 (2011).

[3] "First direct observation of muon antineutrino disappearance." by MINOS collaboration (P. Adamson *et al.*), Phys. Rev. Lett. 107, 021801 (2011).

[4] "Neutrino and Antineutrino Inclusive Charged-current Cross Section Measurements with the MINOS Near Detector." The MINOS Collaboration (P. Adamson *et al.*), Phys.Rev.D81:072002,2010.

[5] 'Search for the disappearance of muon antineutrinos in the NuMI neutrino beam.", by MINOS collaboration (P. Adamson *et al.*), Phys. Rev. D84, 071103 (2011).

[6] K. S. McFarland [The MINERvA Collaboration], [arXiv:1108.0702 [hep-ex]]; D. Harris, to be published in Proc. of EPS2011, European Physics Society; R. Ransome, to be published in Proc. of PIC2011, Physics in Collision; G. Perdue, to be published in Proc. of NUFACT11.

[7] "The T2K Experiment." by the T2K Collaboration, Accepted for publication Nucl. Instrum. Meth. A. (2011), arXiv:1106.1238 [hep-ex]

[8] "Indication of Electron Neutrino Appearance from an Accelerator-produced Off-axis Muon Neutrino Beam." by the T2K Collaboration, Phys. Rev. Lett. **107**, 041801 (2011) [arXiv:1106.2822 [hep-ex]].

TASK L: ATLAS PROGRAM AT CERN

Between November 2008 and May 2012, Task L supported Pitt's ATLAS group which included co-PIs J. Boudreau, J. Mueller, V. Paolone (until 2011), and V. Savinov. W. Cleland (emeritus, not supported by the grant) continued to be involved in our electronics efforts. During this time, the group has supported 5 graduate students: V. Bansal (graduated in August 2009), S. Wendler

(graduated in September 2010) R. Yoosoofmiya (expected to graduate in December 2012) K. Sapp (joined the group in 2009, expected to graduate in 2013), and J. Su, who joined the group in May 2012. Two software professionals stationed at CERN have worked with the group V. Tsulaia (supported by a DOE subaward from BNL) worked with Boudreau on core software. T. Kittleman (supported over time by various sources) worked with Boudreau on VP1, the 3-D ATLAS event display. Three Postdoctoral associates worked with the group. D. Prieur (supported primarily by an NSF subaward from Columbia University), stationed at CERN, was our key off-site personnel responsible for our electronics commitments to Liquid Argon collaboration and ATLAS. Due the nature of his support, he initially worked solely on this task. As funds for partial support for Prieur became available in Task L, he was able to begin to collaborate with Savinov on searches for exotic physics. C. Escobar was hired in 2011. Initially, he worked on maintaining VP1 and collaborated with Boudreau and Mueller on top-quark studies. B. Akgun was hired in 2012 to replace Prieur, but budget reductions in the succeeding grant to this one forced us to terminate that position. Escobar then assumed duties related to our commitment to Liquid Argon electronics, while maintaining his physics analysis efforts.

Over the past few years we contributed to ATLAS in the areas of integration of the LAr electronics and software with the rest of ATLAS, core software and geometry description, VP1 event display, detector simulation, MC generators, validation, detector performance studies, calibration of b-tagging algorithms, and data analysis.

Boudreau's and Mueller's primary physics interests with the LHC lie in the area of heavy flavors, first of all t quark physics. Savinov's interests are primarily in the area of exotic processes that can help explain the nature of light neutrinos and their masses. Savinov and Paolone collaborated on a GUT physics analysis performed by Wendler, where she searched for leptoquarks in dimuon+jets channel, which was the subject of her PhD analysis. Bansal's PhD thesis focussed on leptoquark discovery in dielectron+jets channel. Yoosoofmiya's PhD work includes a search for heavy neutrinos with 2011 data.

9 Trigger Electronics

Cleland (Professor Emeritus), Paolone and Savinov collaborated on designing and building the front-end and trigger electronics for ATLAS calorimeters. We built the Layer Sum Boards (LSBs) which are small daughterboards installed on the Front-End Boards (FEBs) of front-end crates of Liquid Argon (LAr) calorimeter. Their function is to perform the analog sums of FEB channels that are within the same trigger tower. The circuit adds negligible noise to the output and is linear up to the point where it saturates. The receiver/monitoring system we designed and built in Pittsburgh is the interface between all ATLAS calorimeters and calorimeter-based L1 trigger. This system has four basic functions:

- to prepare the signals for transmission to the L1 preprocessors, where they are digitized,
- to carry out two-fold sums of signals which are coming out of two independent sub-detectors (EMB and EMEC) but lie within the same trigger tower (such summing is also being used to reduce granularity of forward calorimeter (FCAL)),
- to change the order of the signals at the input, which is dictated by the cabling in the calorimeter and front-end crates, to one at the output, which is needed for the L1 trigger processor and
- to monitor analog trigger sums of the calorimeters.

During the funding period described in this report our group was responsible for all aspects of the integration, performance and maintenance of the Receivers/Monitoring system and LSB boards. To fulfill our responsibilities to LAr and ATLAS Prieur and Yoosoofmiya were stationed at CERN (these responsibilities are now carried by Escobar and Su). Tasks included support for custom USB firmware and software (for technical reasons we use VME single-board computers that are not used anywhere else on ATLAS). While our system is TDAQ-compliant, we were responsible for keeping our modules and real-time software up-to-date. We were responsible also for monitoring of LAr trigger towers, calibration of their relative and absolute gains for the L1 trigger, and studies of relative timing and signal shapes for presampler and the three layers of LAr.

10 Detector Description, Simulation, and Event Display

The Pittsburgh group has contributed a number of important pieces of software infrastructure to the ATLAS experiment. Fig. 6 is an event display of the Higgs boson candidate recorded at ATLAS in summer 2012. The illustration helps us summarize the main contributions of the Pitt ATLAS group to software infrastructure:

1. The Pittsburgh group developed an API called GeoModel used to express the complicated geometry of the ATLAS detector and supervised the retrofitting of all ATLAS simulation and reconstruction code to the GeoModel in the pre-datataking period.

2. The Pittsburgh group developed the VP1 Event display program from scratch during a two year period (2007-2009) using funds from USATLAS software and computing.

GeoModel is a detector modeling toolkit that consists of geometrical primitives and transformations. The primitives and transformations can be assembled in a acyclic graphs. These acyclic graphs encode a hierarchy of geometrical structures containing nested coordinate systems ("local coordinates"). "Detector Elements" are special volumes that require a cache of alignment information and the possibility of further customization (silicon strips, calorimeter cells, etc.). "Alignable transforms" are special transformations allowing adjustments to the position of the whole subtree of daughter volumes. To save memory, the system provides for shared instancing of identical volumes in addition to a computer algebra layer for constructing expressions for the placement of volumes. In ATLAS, the geometry is expressed in a neutral way that is appropriate for simulation or reconstruction. In simulation, the model is constructed, translated to Geant4, and then mostly deconstructed to save memory. Only the active volumes persist in memory, for as they may be used during hit production and/or digitization. The system was developed by Boudreau and Tsulaia and has been in continuous use in ATLAS since its introduction, during which time it has required relatively little maintenance. The Pittsburgh group wrote the GeoModel toolkit, but also the conversion utility to transform GeoModel to Geant4, and the relational database used to store and version the detector geometry, and the layer to retrieve specific versions. We also wrote the interactive database browser allowing to create and browse collections of database constants used to store specific geometry configurations. Tsulaia was the chief administrator of this database and insured that it was properly replicated to central and remote sites.

The conversion of the ATLAS software to a GeoModel description was a major task involving the software of all subdetectors. Boudreau was head of the detector description project during the years when this activity took place, and successfully prepared all of the detector description software for the first big Geant4-based simulation runs. The Liquid Argon detector was one of the last subsystems to convert. Boudreau served as leader of the liquid argon simulation, where the

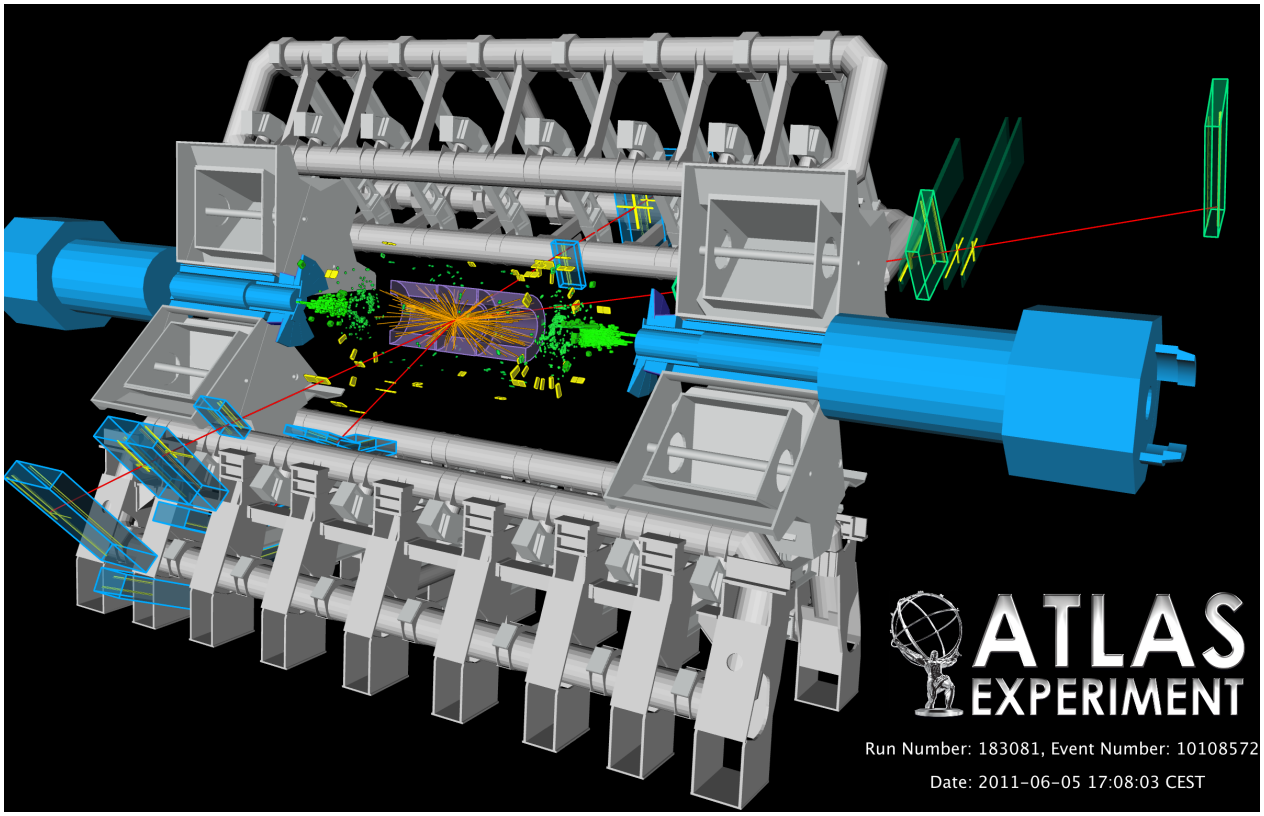

Figure 6: An event display of a $H^0 \to Z^0 Z^0 \to \mu^+\mu^-\mu^+\mu^-$ candidate at ATLAS. The figure illustrates some of the Pittsburgh past and present software responsibilities. 1) We are responsible for the GeoModel toolkit which is used to express the geometry of the ATLAS detector. 2) We organized, as detector description coordinator, a complete rewrite of all detector subsystem geometry to use GeoModel. 3) we lead the liquid argon calorimeter simulation effort, as well as an effort to develop frozen shower libraries as to optimize the simulation, and finally, 5) we developed the VP1 event display program used to make this image.

major task was to integrate the liquid argon with the atlas analysis framework (athena) and with the GeoModel, while preserving several test beam configurations.

The full GEANT4 simulation of the calorimeters is essentially a complete project, with many users depending on calorimeter simulation in one way or another. In the past years, Joe Boudreau and Vakhtang Tsulaia, working with partners at other institutions, have striven to make this simulation compliant with the ATLAS detector description (GeoModel), to make the software description alignable, to drive the simulation more and more from databases, to add geometric realism, to adapt the simulation to emerging protocols ("pythonizing") for steering the simulation, to fully describe four test beam simulations of ATLAS in addition to full ATLAS, to maintain and extend the types of Monte Carlo truth information recorded during simulation. The last major effort we undertook , and completed, was to incorporate pathologies related to high voltage imperfections in the simulation. Our involvement with LAr simulation has essentially ended when Vakho Tsulaia left the group in 2011.

Thomas Kittelmann, who was supported through project funds through March 2009, was devoted 100% to the VP1 event display effort. This effort did not receive dedicated funding in the previous grant period; however the VP1 event display program has continued to function with a

significant user base throughout the current data-taking period. As a scientific instrument it continues to serve as a primary tool for debugging reconstruction software, particularly tracking software, and its interactive 3D geometry browser makes it a critical tool for defining the geometry of new detectors, particularly those due for installating during the LHC's long shutdown period. And, as Fig. 6 illustrates, it has provided a plethora of striking images of LHC events that now adorn the covers of textbooks and physics journals in addition to appearing all over the popular media.

VP1 is based on industry-standard technologies: the Qt Toolkit for a graphical user interface, and the Coin/OpenInventor graphics library for fast, hardware-accelerated real time rendering. It directly accesses the ATLAS event store and/or detector store, which enables it to use the ATLAS data itself as input. It runs within the athena framework and provides a framework-within-a framework, enabling developers to write graphics plug-ins to VP1. All settings can be saved after a session, allowing users to restore their sessions along the lines of an edited document. The program is highly engineered and therefore fairly simple to maintain and extend.

10.1 Fast Shower Parameterization

The simulation of a $Z \rightarrow e^+e^-$ event in ATLAS takes approximately 1/2 hour when particles out to $\eta < 6$ are fully simulated on a 2.4 GHz Pentium IV processor. This time can only be described as excessive. As a result, the compute model for ATLAS currently estimates being able to generate samples of full simulation equal to only 20% of the actual data collected by the detector. It is imperative that the full simulation be made substantially faster, with minimal loss of accuracy. The CPU is spent mostly in the simulation of the calorimeter, where the full GEANT4 tracking and simulation of physics processes are thrown at the problem. A fast shower parameterization of transverse and longitudinal shower shapes was implemented by our colleagues from the University of Melbourne in Australia. We integrated this model into the simulation and benchmarked it on a farm of processors. While the method showed substantial speed improvements for high energy electrons entering the calorimeter, we showed that the improvements were much less dramatic for electrons generated at the interaction point. Due to the large amount of material in the inner detector of ATLAS, electrons will begin to shower inside the tracking system. By the time a high energy electron reaches the calorimeter, it is accompanied by a halo of low energy electrons and positrons. These low energy particles dominated the simulation time. Based on this, our colleagues at DESY developed a library of frozen showers which we implemented inside the full simulation. This library replaces full GEANT for low energy electrons (< 1 GeV) over all the LAr calorimeters.

The use of frozen showers substantially increased the speed of the simulation of high energy electron showers. Except for the regions between detectors, our benchmarks showed there is over an order of magnitude improvement in cpu time. However, full events showed less impressive gains, typically only a factor of 2-3. The current diagnostics were insufficient to show where the difference was coming from. Mueller and Sapp, a new graduate student, decided to develop a more detailed diagnostic, in order to see where to make further improvements. Although work is still ongoing, one dramatic effect was observed. Approximately 40% of the GEANT4 time was being spent stepping low-energy neutrons through the detector. Working with colleagues, we determined methods for drastically reducing this time, without introducing biases in the simulation. At present, frozen showers are deployed in ATLAS in the forward calorimeters where the method has been sufficiently validated. More work will be required to deploy the method in the endcap region where more large gains can be anticipated.

10.2 MC Generators

Until Spring 2012 Savinov and Yoosoofmiya were involved in many aspects of work of ATLAS MC generators working group. Savinov was responsible for several interfaces between individual MC generators and ATLAS offline software framework (ATHENA) and the performance and suitability of these generators for ATLAS purposes. The areas of responsibility invluded interfaces to PHOTOS, TAUOLA and COMPHEP. Also, Savinov and Yoosoofmiya contributed to various performance studies and troubleshooting of PYTHIA, HERWIG and MC@NLO. In a collaboration with Savinov's former PhD student, Bansal, an important problem was diagnosed in PYTHIA. Problems were found and diagnosed in HERWIG and its treatment of polarization in exotics processes. Major efforts were made to change the algorithms of using PHOTOS and TAUOLA on ATLAS making it possible to use these generators in the first place in more recent ATLAS offline software releases. The group was also involved in MC production for Exotics WG, numerous validations and quality control projects. The involvement in MC generators group came to an end in Spring 2012.

11 Exotic Physics

During the reported funding period Savinov, Prieur, Bansal, O'Connell, Wendler and Yoosoofmiya were involved in several analysis efforts in the framework of Exotics Working Group (WG) and its Leptons+X and Diboson subgroups. Savinov collaborated with Budker Institute of Nuclear Physics (BINP) on a search for heavy neutrinos and W_R. Together with Anyes Taffard from UC at Irvine he co-edited a conference note (which later became a journal publication [1]) on this subject. The group was also involved in the inclusive search for Beyond-the-Standard-Model (BSM) physics in final states with two same-sign leptons of high transverse momenta. Together with Wendler (defended her PhD in 2010), O'Connell (left the group) and in collaboration with Bansal (now at University of Victoria), we contributed to the first ATLAS search for leptoquarks. Finally, Prieur, Yoosoofmiya and Savinov participated in studies of isolation energy and lepton identification efficiencies for the first ATLAS Z' analysis.

During the past funding period we used data from 7 TeV pp collisions recorded with the ATLAS detector [2] in 2010 and 2011 to investigate several BSM scenarios with dileptons. First of all, we were involved in the search for heavy neutrinos and W_R using both same-sign (SS) and opposite-sign (OS) dileptons (including the cross-flavor channel) and up to two hadronic jets. We pioneered the search for the W_R in its decays to heavy neutrinos on ATLAS, were responsible for all aspects of this analysis and got our collaborators from BINP, Uppsala and, at a later time, several other groups involved in this effort. In fall of 2010 this analysis effort was merged with the inclusive search for heavy neutrinos (where the scale of BSM is assumed to be far above LHC reach) led by Anyes Taffard from UC at Irvine. We then collaborated with her group.

Another effort we were involved in, the inclusive search for BSM with SS dileptons, was not focusing on a particular model. While sensitivity of this analysis is not optimal for any of the BSM physics scenarios, early on we suggested to use Left-Right Symmetry as a benchmark for the inclusive SS study, so the choices made in this analysis had been influenced by our proposal. We contributed to various MC and data-based studies for the inclusive analysis and were one of the three groups who performed the detailed comparisons of the events selected for the final analysis. We played a leading role in studies of isolation energy, which allowed to improve BSM sensitivity after we proved (using the data) that a sizable QCD background remains in the sample after the back-then final selection. Our closest collaborators in this effort were Daniel Whiteson (UC at Irvine) and Michael Wilson (SLAC).

Until summer of 2011 we were also working on leptoquarks (Bansal and Wendler, former stu-

dents, both defended their PhD theses on the subject) and contributed to the first leptoquark search with ATLAS data in the final state with dileptons and dijets. Our notable contribution, in collaboration with Bansal, is the study we performed in 2011 to convince our ATLAS colleagues that Pt-based parton showering implemented in PYTHIA a few years earlier does not handle colored objects properly, which results in QCD showers being generated in the directions of final state leptons coming from the decays of leptoquarks. This study was important for understanding lepton identification efficiency that was unreliably predicted by MC simulation for the signals. The problem was diagnosed, understood, reported to PYTHIA authors and a solution was found. The results of our study were significant, because they affected ATLAS estimates of limits on leptoquark masses and production cross sections.

Our contribution to the Z' studies based on 2010 data had been limited, as this work was performed in a large collaboration of many ATLAS groups. We mainly focused on calorimeter and the inner detector-based isolation energy parameters, their comparisons between data and MC and the measurements of the efficiencies of selection criteria based on isolation energy measurements. We were responsible also for prompt retrieval of the interesting individual events from data and preparing data for event displays.

Below we describe the four analysis efforts we contributed to. Our major involvement was the search for possible effects of Left-Right Symmetry (LRS) in ATLAS data. Our contribution to the other described analyses was less significant, as a number of other US and foreign groups collaborated to obtain the results we are reporting.

11.1 Analysis Objects

In all four analyses we used (with small variation) almost the same selection criteria for leptons and, where applicable, for jets. In our studies we employed the standard ATLAS selection[3] for high-pt electron and muon candidates. Electrons were required to satisfy the so-called "medium" selection criteria, with $p_T > 20$ GeV and pseudorapidity $|\eta| < 2.47$, excluding the barrel-endcap transition region of the electromagnetic calorimeter, $1.37 < |\eta| < 1.52$. In order to suppress electrons arising from photon conversion, reconstructed trajectories (tracks) of electron candidates passing through the active region of the innermost pixel detector were required to include a measurement in that layer. Electrons whose Inner Detector (ID) track segments also matched that of a muon candidate were rejected.

Muons were required to be identified either in both ID and Muon Spectrometer (MS) or via a match between an extrapolated ID track and one or more segments in the MS. The ID track was required to include at least one pixel hit, more than five Semi-Conductor Tracker (SCT) hits, and an η-dependent number of hits in the Transition Radiation Tracker (TRT). For muons, a good match between ID and MS tracks was required, and the p_T values measured by these two systems were required to be consistent with each other within the resolution. Muons were required to have $p_T > 20$ GeV and $|\eta| < 2.4$. For the final selection, the distance between the z coordinate of the primary vertex and that of the extrapolated muon track at the point of closest approach to the primary vertex was required to be less than 5 mm, while the distance in $r\phi$ was required to be less than 0.2 mm.

To reduce the background due to leptons from decay of hadrons (including heavy flavor particles) produced in jets, the leptons were required to be isolated. For electrons, the energy deposited in the calorimeter towers in a cone in $\eta - \phi$ space of radius $\Delta R = 0.2$ around the electron position[1] was summed and corrected for energy leakage. An equivalent quantity was calculated for the muon using the same cone size. The E_T energy in this cone was required to be less than 15% of the

[1] ΔR between the object's axis and the edge of the object's cone was defined as $\Delta R = \sqrt{\Delta\phi^2 + \Delta\eta^2}$.

electron's E_T or muon's p_T. Additionally, muons within $\Delta R < 0.4$ of a jet with $p_T > 20$ GeV or of a candidate electron were rejected.

Jets were reconstructed using the anti-Kt jet clustering algorithm [4, 5] with a radius parameter $R = 0.4$. The inputs to this algorithm were clusters of calorimeter cells seeded by cells with energies significantly above the measured noise. Jets were constructed by performing a four-vector sum over these clusters, treating each cluster as an $(E,\vec{p})$ four-vector. Jets were corrected for calorimeter non-compensation, upstream material and other effects using p_T and η-dependent calibration factors obtained from MC and validated with extensive test-beam and collision-data studies [6]. Only jets with $p_T > 20$ GeV and $|\eta| < 2.8$ were considered. The closest jet to a candidate electron within a distance $\Delta R < 0.5$ was discarded. Events were also discarded if they contained a jet failing basic quality selection criteria, which rejected detector noise and non-collision backgrounds [7].

Events were required to have at least one reconstructed primary vertex with at least five associated tracks. At least one of the lepton candidates was required to match a triggered lepton at the last stage of the trigger selection.

In the rest of this section we describe the four analysis efforts we collaborated on with a number of ATLAS groups and individuals. All described studies employed baseline selection criteria described above. Our work was based on our own source code we designed and developed to perform the analysis at Analysis Object Data (AOD) and Event Summary Data (ESD) levels.

11.2 Heavy Neutrinos and Left-Right Symmetry

The discovery [8] of large mixing between the second and the third generations in the light neutrino sector unambiguously established that neutrinos have finite masses and offers one of the most compelling indications of physics beyond the Standard Model (SM). A mass generation mechanism for the known neutrinos can be realized with one or more additional neutrino fields, that could manifest themselves as new particles directly observable at the LHC. The masses of the light neutrinos could be explained via the seesaw mechanism [9], which results in $m_\nu \approx m_D^2/M_N$, where, for each generation, m_ν is the mass of a known light neutrino, m_D is the Dirac mass term for charged fermions of the same generation, and M_N is the mass of the new heavy neutrino. If the seesaw mechanism was to explain the masses of the known neutrinos, all neutrinos would have to be Majorana particles yielding (50% of the time) a striking signature of SS dileptons therefore violating lepton number conservation. However, if LRS realizes at LHC energies but does not explain the masses of light neutrinos via the seesaw mechanism, only OS signal would be observed. Therefore, the search has to be performed in both SS and OS channels. Further, there could be mixing in heavy neutrino sector, so final states with dileptons of different flavor should be analyzed.

In our original analysis we searched for the new intermediate gauge boson W_R and heavy Majorana neutrinos, N, with data corresponding to an integrated luminosity of 34 pb^{-1}, recorded with the ATLAS detector in 2010. At a later time we extended our analysis to include 2011 data. Two complementary approaches were employed in both analyses. UC at Irvine group lef by Taffard aimed at exploring possible sources of new physics generating the seesaw mechanism using a Lagrangian of effective operators (referred to as HMN hereafter) [10]. Since the theory is built on effective operators, it allows probing any new physics that would lead to the existence of heavy Majorana neutrinos, however, the theory says nothing about the new gauge couplings and the origin of BSM particles. The production process considered is that of $q\bar{q} \to Nl^\pm$, where N decays promptly as $N \to l^\pm jj$ via a three-body decay described by an effective operator. The other approach, pioneered by our group, was guided by the idea of LRS (and its model implementation, LRSM) and is not limited to Majorana neutrinos. LRS introduces a new gauge group with its force particles (W_R and Z_R) possibly manifesting themselves directly at LHC energies [11]-[13]. In this approach, the

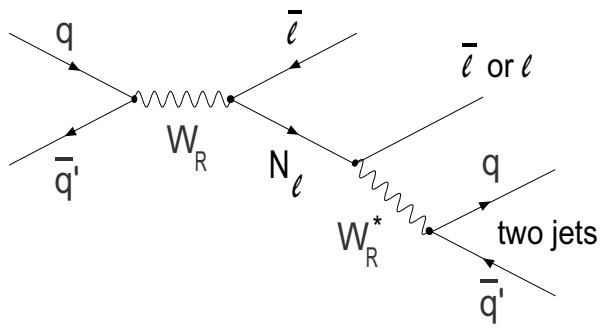

Figure 7: Feynman diagram for heavy neutrino production in the decays of W_R. Mixing among heavy neutrinos could be present resulting in dileptons of different flavor. In particular models of LRS breaking neutrinos are Majorana particles that could also exhibit direct CP violation measurable by comparing the rates for SS and OS dileptons in W_R decays. Such CP violation could be sufficient to satisfy relevant condition for baryogenesis.

heavy neutrinos N are produced in the decays of a W_R via $q\bar{q} \to W_R \to lN$, with N decaying subsequently to $N \to lW_R^* \to ljj$ as Feynman diagram in Fig. 7 demonstrates. The final state signature for both models is two high transverse momentum (p_T) leptons (electron or muon) and two high-p_T jets (though these could be detected as one jet, when they are Lorentz-boosted in the decay of heavy neutrino that comes from a much heavier W_R). The N and W_R invariant masses can be fully reconstructed from the decay products. If the heavy neutrinos are of Majorana type, they would contribute to both the SS and OS channels, while non-Majorana heavy neutrinos would contribute solely to the OS channel. The OS final state can be exploited for the LRSM since the expected signal events, for the considered W_R masses, contribute to the tail of the kinematics of SM events. This is not the case for the HMN signal with low N mass, for which the decay spectrum is softer. Thus, only the SS final state is considered in the case of the HMN search.

Heavy neutrinos had been previously searched for at LEP [14, 15] and were excluded for masses up to ≈ 100 GeV. The most stringent direct limits on the W_R bosons come from the Tevatron, which excluded W_R with masses below 739 GeV, if the W_R boson decays to either leptons or quarks [17]. To search for W_R and heavy neutrinos, in addition to the already described baseline selection criteria, we required exactly two identified leptons with $p_T > 20$ GeV originating from the primary vertex and at least one jet with $p_T > 20$ GeV. In order to reduce the number of background events from Drell-Yan processes and misidentified leptons, the dilepton invariant mass, m_{ll}, is required to be larger than 110 GeV. The signal region is then subdivided into SS and OS dilepton events. The event selection efficiency for the HMN signal varies between 5.4% for $m_N = 100$ GeV and 9.7% for $m_N = 500$ GeV, while it varies widely for the LRSM signal depending on the mass of W_R and the mass ratio between W_R and N. In a search for W_R, the improved sensitivity is achieved with additional optimization requirements. The W_R invariant mass, reconstructed from the leptons and up to two leading p_T jets, m_{lljj}, is required to be at least 400 GeV. To further reduce larger SM background contributions in the OS dilepton channel, the scalar sum of the transverse energies of the leptons and up to the two highest p_T jets, S_T, is required to be larger than 400 GeV.

The numbers of observed data events and the expected SM background events in the signal regions with $m_{ll} > 110$ GeV for the SS and OS final states are shown in Table 1. For the HMN analysis, 5 data candidates are observed which agrees with the SM expectation of $7.1 \pm 1.4(\text{stat.}) \pm 2.1(\text{sys.})$. The reconstructed N mass, m_{ljj}, from the sub-leading lepton and up to two leading jets is shown in Fig. 8. Kinematic distributions of the dilepton-dijet invariant mass and S_T in the OS final state prior to the selection criteria on those variables are compared to the SM expectation in Fig. 9. For both distributions, a good agreement between the data and the predicted background is observed. For the LRSM analysis in the SS dilepton final state, after the additional requirement on $m_{W_R} > 400$ GeV, the SM background expectation is $1.8 \pm 0.5(\text{stat.}) \pm 0.6(\text{sys.})$ while 2 data candidates are observed. For the OS final state, after all additional requirements, including $S_T >$

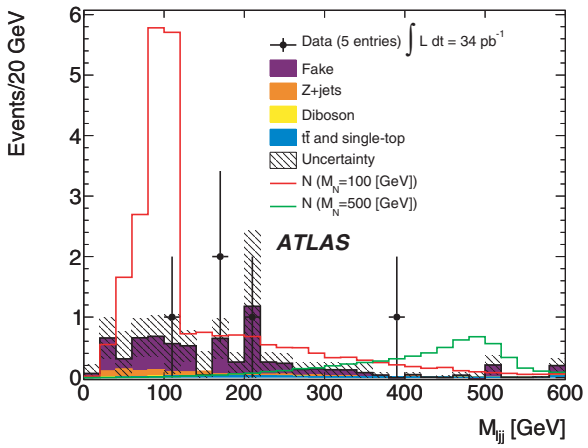

Figure 8: Distribution of the invariant mass of the sub-leading lepton and up to the two leading jets for SS dilepton events with at least one jet and $M_{ll} > 110$ GeV. The signal distributions for $m_N = 100$ GeV and $m_N = 500$ GeV are also shown.

400 GeV, 10 data candidates are observed, in good agreement with the SM background expectation of $13.6 \pm 1.2(\text{stat.}) \pm 2.0(\text{sys.})$. Fig. 10 shows the distribution of m_{lljj}, the reconstructed W_R mass in the SS and OS final states after all selection criteria are applied. In all figures and the table *flavor fakes* (or *fake leptons*) represent lepton background contribution from decays of hadrons or heavy quarks. This notation is chosen because the true flavor produced by the interaction is a quark flavor (typically b or c), which leads to a jet in the detector. Fake leptons are usually poorly isolated.

Physics Processes	SS	OS
Diboson	$0.06 \pm 0.01 \pm 0.01$	$4.0 \pm 0.1 \pm 0.4$
$t\bar{t}$ + single top	$0.39 \pm 0.01 \pm 0.06$	$56.6 \pm 0.6 \pm 8.0$
$Z \to ll$	$0.81 \pm 0.06 \pm 0.15$	$109.7 \pm 3.2 \pm 14.0$
Flavor fakes	$5.81 \pm 1.37 \pm 2.13$	$6.9 \pm 2.3 \pm 2.7$
Total background	$7.1 \pm 1.4 \pm 2.1$	$177.2 \pm 4.0 \pm 17.1$
Observed in data	5	177

Table 1: The background predictions and the observed numbers of events for the SS and OS dilepton events with at least one high-pt jet and $m_{ll} > 110$ GeV. For each background estimate, the first and second uncertainties are of statistical and systematic origin, respectively. The uncertainty due to the luminosity (not included) is 3.4% for all backgrounds except for the non-isolated leptons, which is measured from data by our collaborators from UC at Irvine.

Using 2010 data we estimated upper limits on the cross-sections times branching ratios for new physics based on the HMN and the LRSM models. To do so classical confidence intervals for the theoretical cross section were constructed by generating ensembles of pseudo-experiments that describe expected fluctuations of statistical and systematic uncertainties on both signal and backgrounds, following the likelihood ratio ordering prescription proposed by Feldman and Cousins [18]. For the LRSM model, the W_R resonance peak reconstructed from m_{lljj} is used to set the limits on the total production cross section times branching ratio to $ee, \mu\mu$ for the no-mixing scenario (Fig. 11) and to $ee, \mu\mu, e\mu$ for the maximal mixing scenario between N_e and N_μ (Fig. 12). The limits are presented as a function of the W_R and N masses and determined separately for SS events and SS+OS events. A large fraction of the mass parameter space is excluded, where the addition of the OS events improves the limits significantly. Those limits surpass previous limits set by other

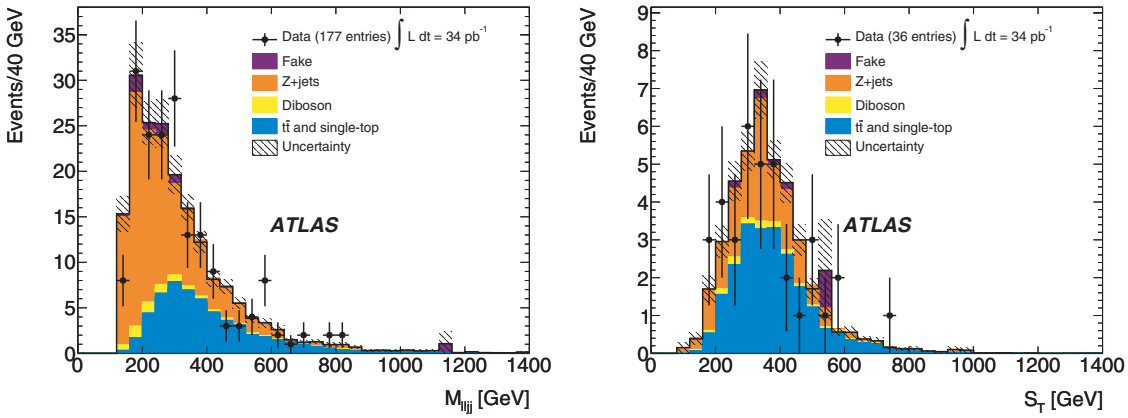

Figure 9: On the left is the distribution of the dilepton-dijet invariant mass, M_{lljj}, for OS dilepton events with at least one jet after $M_{ll} > 110$ GeV selection is applied. To be included in the final analysis the events must pass the $M_{lljj} \geq 400$ GeV requirement. On the right is the distribution of S_T for OS dilepton events with at least one jet after $M_{ll} > 110$ GeV and $M_{lljj} \geq 400$ GeV selection criteria are applied. To be included in the final analysis the event must satisfy the requirement $S_T \geq 400$ GeV.

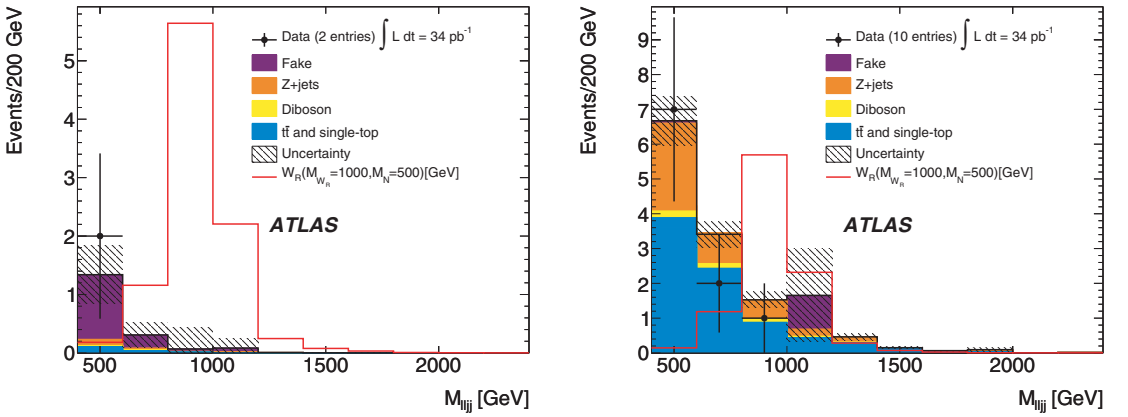

Figure 10: Distribution of the dilepton-dijet invariant mass, M_{lljj}, for SS (left) and OS (right) dilepton events with at least one jet after $M_{ll} \geq 110$ GeV and $M_{lljj} \geq 400$ GeV selection. In addition, OS dilepton events must satisfy $S_T \geq 400$ GeV. Overlaid is the signal distribution predicted by LRSM for $m_{W_R} = 800$ GeV and $m_N = 300$ GeV.

experiments [14]-[17].

In 2011 and 2012 we analyzed 2011 data and improved the analysis that was eventually published. [1]

11.3 Inclusive Same-Sign Dileptons

A diverse group of models, not limited to heavy neutrinos and LRSM, predict interactions producing two leptons of the same electric charge and with significant transverse momentum – a signature quite

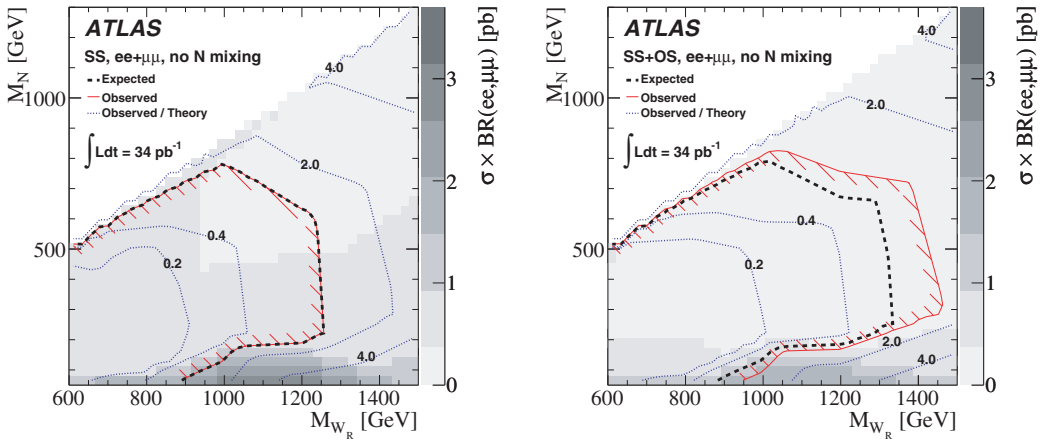

Figure 11: Observed and expected 95% CL upper limits on cross-section times branching fraction as a function of the heavy neutrino and W_R masses in the no-mixing scenario for SS events (left) and SS+OS events (right). The excluded region is inside the solid-hatched boundary. The contours show the ratio of the 95% CL exclusion to the theory prediction.

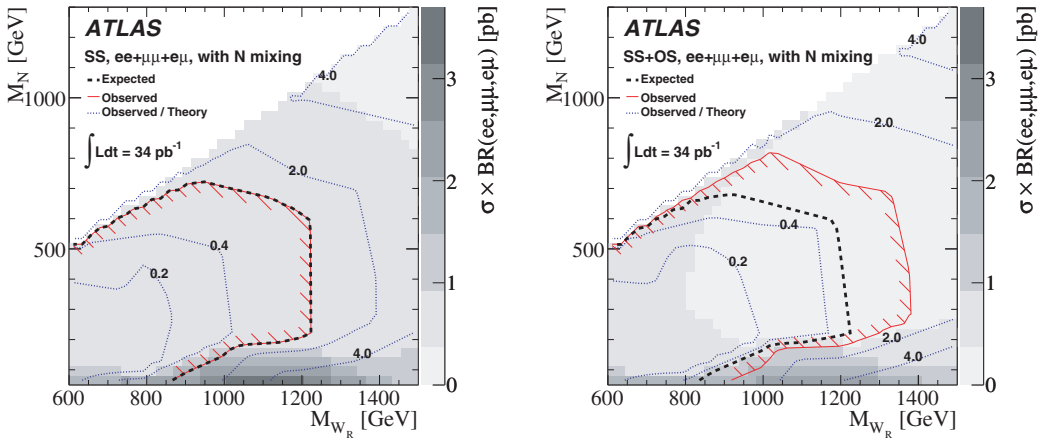

Figure 12: Observed and expected 95% CL upper limits on cross-section times branching fraction as a function of the heavy neutrino and W_R masses in the maximal mixing scenario for SS events (left) and SS+OS events (right). The exclusion region is inside solid-hatched boundary. The contours show the ratio of the 95% CL exclusion to the theory prediction.

rare in the SM. In this analysis we selected SS dilepton events (ee, $e\mu$, $\mu\mu$) inclusively. Previously, similar inclusive analyses by the CDF collaboration [19] produced 95% confidence limits using up to $1\,\text{fb}^{-1}$ of $p\bar{p}$ collisions at a center-of-mass energy of 1.96 TeV. The CMS and CDF collaborations searched for fourth-generation d-type quarks in 34 pb^{-1} of pp collisions [20] and in $2.7\,\text{fb}^{-1}$ of $p\bar{p}$ collisions [21], respectively. They set lower mass limits of 361 GeV and 338 GeV respectively, at 95% confidence level. As we discussed previously, a search by the D0 collaboration excluded W_R

with masses less than 739 GeV in LRS models [16, 17]. Various other specific searches have been performed with SS dileptons [22, 23].

In our work we measured spectra of dilepton invariant mass ($m_{\ell^+\ell^-}$), jet multiplicity (N_{jets}), and missing transverse momentum ($\not{E}_T$)[2] and studied their consistency with the SM to search for evidence for new physics. The SM prediction was estimated by extrapolation from data control samples, with some information from MC simulation. In a kinematic fiducial region, an upper limit on the cross-section of high-mass ($m_{\ell^+\ell^-} > 110$ GeV) same-sign dilepton events from non-SM sources was measured for each channel, and benchmark selection efficiencies for some specific models were provided.

SM processes could produce SS dileptons in three ways. True SS dilepton events are produced from SM diboson processes, most notably from WZ production. These are a rare but irreducible background to new physics sources, since events with more than two leptons are not excluded in the inclusive analysis. Such SM SS dileptons are distinguishable from BSM only by differences in kinematic spectral shapes on statistical basis.

When a lepton is produced inside a jet, therefore being poorly-isolated, such lepton represents a flavor fake. Processes that are often reconstructed as SS dileptons in this way are quantum-chromodynamical (QCD) dijet production and final states with a W-boson and jets. This is the main background considered in this analysis as it has the largest overall contribution to the sample. It is dominant in the $\mu\mu$ and $e\mu$ channels.

It is also possible to misreconstruct an event as SS dilepton when primary daughters produced with opposite electric charge lead to good same-sign lepton candidates in the detector. Processes susceptible to this effect are $Z/\gamma^* \to e^+e^-$ and $t\bar{t}$ semileptonic decays with at least one electron. This misreconstruction occurs if an electron undergoes bremsstrahlung, and upon conversion the photon passes the larger share of momentum to an electron of the opposite charge. For this reason, this effect is known as *electron charge flipping*. The charge-flip category is dominant in the ee channel and present in the $e\mu$ channel. When the bremsstrahlung does not carry the majority of the electron energy, misidentification of electron charge may occur due to misreconstruction of the ID track. When found in this analysis, such events are included in the charge-flip category. A few years ago Yoosoofmiya performed a detailed analysis of such evens using MC simulation. Recently, we confirmed his finding using the data. Misidentification of muon charge is negligible due to near absence of bremsstrahlung from muons.

To quantify the consistency between the observed yield and the SM prediction we used the Kolmogorov-Smirnov (KS) distance test. We found a good agreement between the observed data and the SM prediction, as shown in Table 2. In this study, to suppress contamination from misreconstructed $Z \to ee$ events, we excluded dielectron events in the region $80 < m_{\ell\ell} < 95$ GeV from the analysis of the $\not{E}_T$ and N_{jets} distributions.

By measuring the yields in ee, $e\mu$, and $\mu\mu$ channels, we found that the observed high-p_T isolated SS dilepton events are in agreement with the SM predictions. In a model-independent statistical analysis of the inclusive sample, no evidence of unknown physical sources of same-sign dilepton events was found either. Considering the dilepton invariant mass spectrum integrated above 110 GeV, we set upper limits on the fiducial cross-section of a new high-mass source at 0.13 (ee), 0.17 ($\mu\mu$) and 0.32 ($e\mu$) pb at 95% CL.

[2]The missing transverse momentum in an event, denoted $\not{E}_T$, is the vector difference between zero and the total transverse momentum, calculated from energy depositions in the calorimeter and momentum measurements from the muon spectrometer for identified muons.

Table 2: Results of KS-distance test for SM prediction. The maximum KS distance and corresponding p-value (in parentheses) are shown for three kinematic distributions presented in this analysis, and one high-mass subset. Statistical and systematic fluctuations are included in the p-value estimation.

Distribution	$\ell\ell$	ee	$\mu\mu$	$e\mu$
m_{ll}	0.11 (86%)	0.42 (24%)	0.34 (77%)	0.82 (6%)
$m_{ll}(> 110$ GeV)	0.77 (16%)	1.00 (9%)	0.85 (35%)	1.33 (16%)
$E_{\mathrm{T}}^{\mathrm{miss}}$	0.27 (65%)	0.58 (17%)	0.42 (58%)	0.98 (5%)
N_{jets}	0.25 (63%)	0.57 (18%)	0.45 (53%)	1.12 (2%)

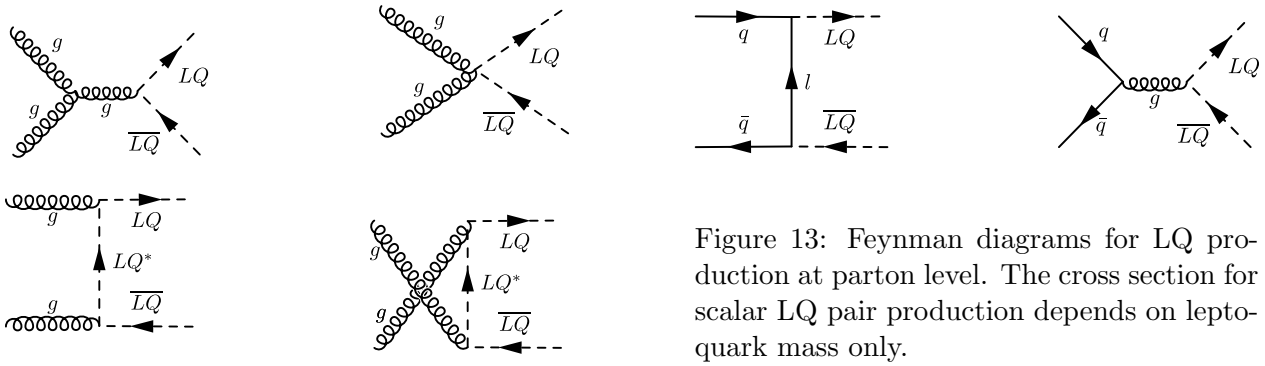

Figure 13: Feynman diagrams for LQ production at parton level. The cross section for scalar LQ pair production depends on leptoquark mass only.

11.4 Leptoquarks

The Standard Model gives no explanation for the striking symmetry between quarks and leptons. This has, in part, been the motivation for many BSM theories that postulate leptoquarks, QCD-colored particles that carry both lepton and baryon quantum numbers therefore coupling to both quarks and leptons. Examples of theories that predict leptoquarks include models that contain quark and lepton sub-structure [24], models that are motivated by the idea of Grand Unification. [25]-[31] and models of extended technicolor [32]. Restrictive experimental bounds on quark flavor-changing-neutral currents and lepton-family-number violation limit leptoquark decays to the same generation of quarks and leptons [33, 34]. Scalar leptoquark production from proton-proton collisions has been calculated to next-to-leading order [35], leading to the expectation that early LHC data could offer sensitivity to a mass range beyond that probed by previous experiments.

By assuming that leptoquarks (LQ) couple to standard model fermions and that their interactions are invariant under Lorentz and the SM gauge group transformations, the quantum numbers and possible interactions of LQs are limited. Both scalar and vector leptoquarks are permitted, as are both chiral and non-chiral LQs. If one assumes the LQ is a scalar, then collider production rates can be calculated as a function of LQ mass only, whereas if one assume the LQ is a vector, production also depends on the coupling strength. At the LHC, a colored LQ would naturally be pair-produced from both gluon-gluon and quark-antiquark interactions, as illustrated in Fig. 13.

While the preferred decay mode of leptoquarks is theory-dependent, the restrictive limits on quark flavor-changing-neutral currents limit leptoquark decays to a specific generation of quarks and leptons [33, 34]. The branching fraction to a charged lepton, (LQ$\rightarrow l$+X), is referred to as β and typically limits are stated either as a function of β or under the assumption that $\beta = 1$.

In our analysis the limits on pair production of scalar leptoquarks are calculated using a binned

modified frequentist approach. The method is described in detail in [36]. Table 3 shows the expected and observed limits as a function of β for the dimuon+dijet channel. The exclusion at $\beta = 1.0$ rules out leptoquarks with $m_{LQ} < 405$ GeV at a 95% CL. Table 4 shows the data event yields in the signal sample after baseline selection (described previously) and successive requirements are applied. No excess of events is observed. Zero $\mu\mu$ events pass all selection criteria, with an expectation of 0.68 events in the absence of a leptoquark signal. Fig. 14 shows a summary of our results, where dilepton-dijet results are combined with the results of a search for LQ pairs, where one LQ decays to a neutrino and a jet.

β	$\mu\mu$ jj Expected (GeV)	$\mu\mu$ jj Observed (GeV)
0.45	257	294
0.5	272	308
0.55	290	320
0.6	304	334
0.65	313	347
0.7	322	356
0.75	333	364
0.8	344	373
0.85	353	382
0.9	396	392
1	372	405

Table 3: Expected and observed limits on leptoquark mass for different values of β.

Cut	Data yield	Background prediction	LQ 300 GeV
$M_{ll} > 120$ GeV	12	13.7	20.7
Avg LQ mass > 150 GeV	1	4.55	19.6
St > 450 GeV	0	0.68	15.7

Table 4: Event yields for data (measured) and for the backgrounds (predicted). The input samples pass the baseline selection for leptons and jets.

In the beginning of 2011 our involvement in leptoquark analysis group started to decline, as the departure of Bansal, Wendler and then O'Connell made it difficult to keep up making timely progress on several analyses simultaneously. We ceased our involvement in leptoquarks in summer of 2011.

11.5 Dilepton Resonances

We also participated in a search for high mass resonances decaying into e^+e^- or $\mu^+\mu^-$ pairs. Among the possibilities for such resonances are new heavy gauge bosons (Z', Z^*) [37, 38, 39]; other hypothetical states include a Randall-Sundrum spin-2 graviton [40] and a spin-1 techni-meson [41], while this analysis is also sensitive to them, these scenarios were not investigated explicitly. The benchmark model for Z' bosons is the Sequential Standard Model (SSM) [37], in which the Z' ($Z'_{\rm SSM}$) has the same couplings to fermions as the Z boson. A more theoretically motivated scenario is the Grand Unification-inspired model in which the E_6 gauge group is broken into $SU(5)$ and two additional $U(1)$ groups [42]. The lightest linear combination of the corresponding two new neutral gauge bosons, Z'_ψ and Z'_χ, is considered the Z' candidate: $Z'(\theta_{E_6}) = Z'_\psi \cos\theta_{E_6} + Z'_\chi \sin\theta_{E_6}$, where $0 \leq \theta_{E_6} < \pi$ is the mixing angle between the two gauge bosons. The pattern of spontaneous

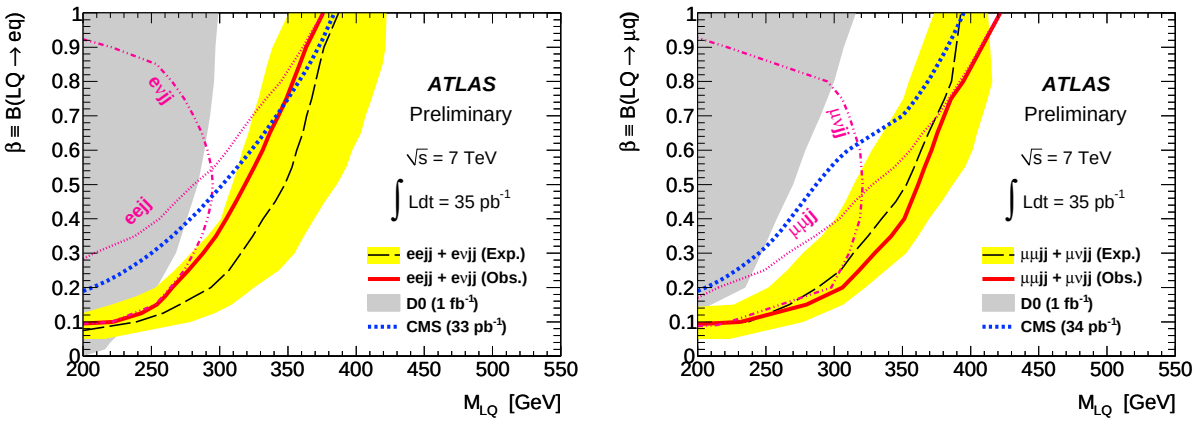

Figure 14: 95% CL exclusion region resulting from the combination of, on the left, the two electron and, on the right, the two muon channels (dilepton-dijet and lepton-$\not\!\!E_T$-dijet) shown in the β versus leptoquark mass plane. The gray area indicates the D0 exclusion limit, and the thick dotted line indicates the (published) CMS exclusion. The dotted and dotted-dashed lines indicate the individual limits for the dilepton-dijet and the lepton-$\not\!\!E_T$-dijet analyses, respectively. The combined expected limit is indicated by the thick-dashed line. The solid band contains 68% of possible outcomes from pseudo experiments allowing Poisson fluctuations of the yield based on the mean background only hypothesis with systematics included. The combined observed limit is indicated by the solid line.

symmetry breaking and the value of θ_{E_6} determines the Z' couplings to fermions; six different models [37, 42] lead to the specific Z' states named Z'_ψ, $Z'_{\rm N}$, Z'_η, Z'_I, $Z'_{\rm S}$ and Z'_χ respectively. Because of different couplings to u and d quarks, the ranking of the production cross sections of these six states is different in $p\bar{p}$ and pp collisions. In this search, the resonances are assumed to have a narrow intrinsic width, comparable to the contribution from the detector mass resolution. The expected intrinsic width of the $Z'_{\rm SSM}$ as a fraction of the mass is 3.1%, while for any E_6 model the intrinsic width is predicted to be between 0.5% and 1.3% [43]. Production of a Z^* boson [39, 44] could also be detected in a dilepton resonance search. The anomalous (magnetic moment type) coupling of the Z^* boson leads to kinematic distributions different from those of the Z' boson. To fix the coupling strength, a model with quark-lepton universality, and with the total Z^* decay width equal to that of the $Z'_{\rm SSM}$ with the same mass, was adopted [45, 46].

Previous indirect and direct searches have set constraints on the mass of Z' resonances [47]-[51]. The $Z'_{\rm SSM}$ has been excluded by direct searches at the Tevatron with a mass lower than 1.071 TeV [52, 53]. The large center of mass energy of the LHC provides an opportunity to search for Z' resonances with comparable sensitivity using the 2010 pp collision data. We note that CMS has excluded a $Z'_{\rm SSM}$ with a mass lower than 1.140 TeV [54].

In our analysis we compared the observed invariant mass distributions, $m_{e^+e^-}$ and $m_{\mu^+\mu^-}$, to the expectation of the SM backgrounds. To make this comparison, the sum of the Drell-Yan, $t\bar{t}$, diboson and $W+$jets backgrounds (with the relative contributions fixed according to the respective cross sections) is scaled such that when added to the data-driven QCD background, the result agrees with the observed number of data events in the 70 - 110 GeV mass interval. The advantage of this approach is that the uncertainty on the luminosity, and any mass independent uncertainties in efficiencies, cancel between the Z'/Z^* and the Z in the limit computation presented below. The integrated Drell-Yan cross section at NNLO above a generator-level dilepton invariant mass of

60 GeV is (0.989 ± 0.049) nb. Fig. 15 shows the invariant mass distributions for dielectrons and dimuons after final selection. The observed invariant mass distributions are well described by the predictions from SM processes. Fig. 15 also displays expected $Z'_{\rm SSM}$ signals for three masses around 1 TeV. Expected Z^* signals (not shown) have a similar shape and approximately 40% higher cross section.

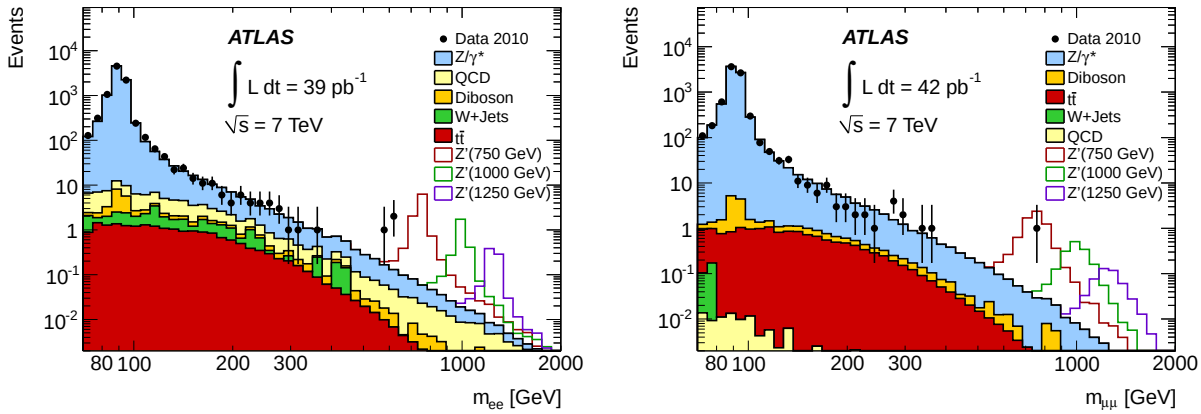

Figure 15: Dielectron (left) and dimuon (right) invariant mass distributions after final selection and the stacked sum of all expected SM backgrounds, with three example $Z'_{\rm SSM}$ signals overlaid.

Three events in the vicinity of $m_{e^+e^-} = 600$ GeV and a single event at $m_{\mu^+\mu^-} = 768$ GeV are observed in the data. The p-value which quantifies, in the absence of signal, the probability of observing an excess anywhere in the search region $m_{\ell^+\ell^-} > 110$ GeV ($\ell = e$ or μ), with a significance at least as great as that observed in the data is evaluated [55]. Since the resulting p-values are 5% and 22% for the electron and muon channels, respectively, no statistically significant excess above the predictions of the SM has been observed. We show event displays for the two highest invariant mass events in Fig. 16. To conclude, we searched for narrow resonances in the invariant mass spectrum above 110 GeV of e^+e^- and $\mu^+\mu^-$ final states with ~ 40 pb^{-1} of proton-proton data. No evidence for such a resonance was found. Limits on the cross section times branching ratio $\sigma B(Z' \to \ell^+\ell^-)$ were calculated, as well as mass limits on the $Z'_{\rm SSM}$ (1.048 TeV), the Z^* (1.152 TeV) and E_6-motivated Z' bosons (in the range 0.738−0.900 TeV). Some of the limits are shown in Fig. 17. For certain E_6-motivated models, these limits are more stringent than the corresponding limits from the Tevatron.

12 Top Quark Physics and Bottom Quark Physics

Boudreau and Mueller have worked together on a program of studies of top and bottom quarks encompassing a variety of short-term and long-term goals. In the first year of ATLAS data analysis we became involved with the calibration of b-tagging algorithms used to separate $t\bar{t}$ production from a background of other QCD processes. As a spinoff of the b-tagging calibration, we have completed an analysis of the b-jet cross section, which can be compared against perturbative QCD calculations and which is an important step in the program of measuring standard model processes at the LHC. The first round of b-tagging calibration is complete with the approval of a conference note on the *system8* method described below, and the calibration of the 2011 datasets was carried out by graduate student Kevin Sapp. We are now involved in an important analysis which measures

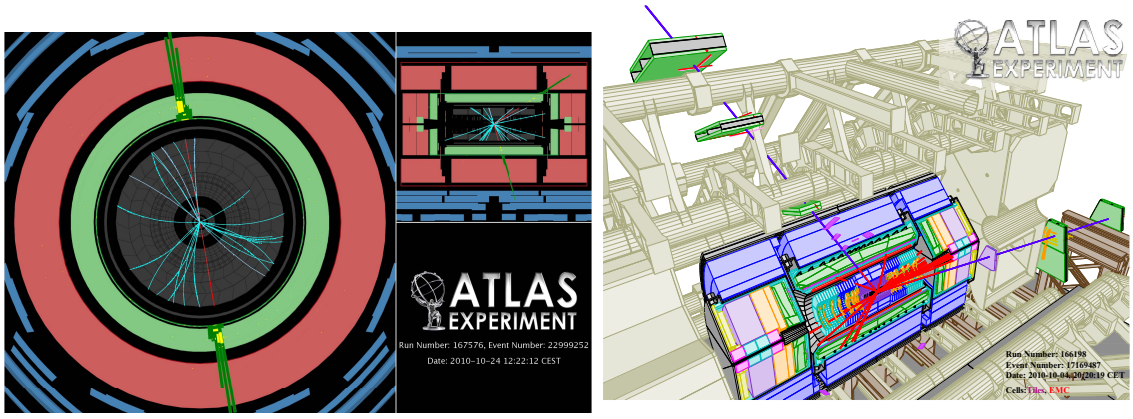

Figure 16: On the left is an event display for the highest invariant mass dielectron event. The leading electron has a pT of 279 GeV and an (η, ϕ) of (1.22, 1.74). The trailing electron has a pT of 276 GeV and an (η, ϕ) of (0.28, -1.40). The invariant mass of the pair is 617 GeV. On the right is an event display for the highest invariant mass dimuon event. The leading muon has a pT of 186 GeV and an (η, ϕ) of (-2.39, -1.54). The trailing muon has a pT of 165 GeV and an (η, ϕ) of (0.46, 1.95). The invariant mass of the pair is 768 GeV. The MET for this event is less than 25 GeV, which indicates the muons are balanced and therefore reconstructed properly.

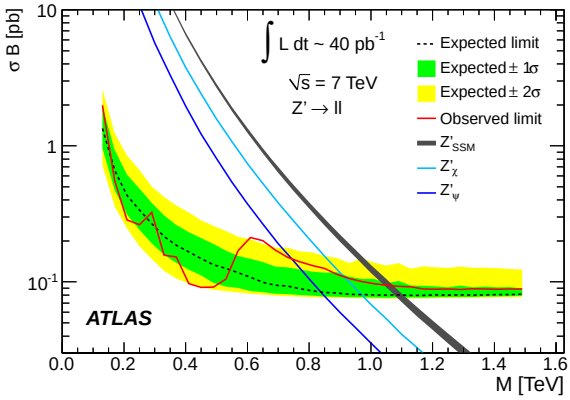

Figure 17: Expected and observed 95% C.L. limits on cross section times branching ratio and expected cross section for the SSM Z' and two of the E6-motivated Z' models shown for the combination of the electron and muon channels. The thickness of the SSM Z' theory curve represents the theoretical uncertainty and applies also to the other theory curves. The curves for the other four E6-motivated Z' models fall in between the ones shown.

top quark anomalous couplings in the single top channel, where top quarks are produced with a high degree of polarization.

Graduate student Kevin Sapp (supervised by Mueller) works on the b-tagging calibration and on the anomalous coupling analysis. Postdoctoral research assistant Carlos Escobar, who joined the group in May 2011, also works on the anomalous couplings analysis in addition to carrying out his hardware responsibilities for calorimeter L1 trigger electronics. Boudreau has recently started working with graduate student Jun Su on the anomalous top quark couplings; however Jun Su is also heavily subscribed to liquid argon calorimeter operations tasks at the moment.

We describe these activities in more detail in the following sections.

12.1 Calibration of *b*-tagging

The identification of jets originating from b-quarks is an important part of the LHC physics program. Of the five lightest quarks (u,d,c,s, and b) only the b-quark can be identified using high-efficiency tagging algorithms. The basis for b-tagging is the displaced track from a b-hadron decay vertex. These tagging algorithms are used to measure both b-jet and top cross sections, and also to search for the Higgs particle decaying into the $b\bar{b}$ final state or any new physics beyond the Standard Model with b-jet signature in the final state.

To obtain the cross section for a final state with b-jets one needs to know the detector's b-tagging performance. In light of this, Boudreau and Mueller have worked on two separate calibration techniques; one using the p_T^{rel} method and one called "*system8*". They are described in the following two subsections.

We have also used the techniques developed for these calibrations to measure the b-jet cross section in ATLAS. This measurement will be described in the subsequent section.

12.1.1 Calibration of *b*-tagging: the p_T^{rel} method.

The development of the p_T^{rel} method is a collaboration between our group, University of Dortmund, CPPM, University of Mainz , and Stockholm University. The analysis uses the momentum of the muon relative to the jet axis, p_T^{rel}, which is given by

$$p_T^{rel} = p_\mu \cdot \sin\theta^{rel}, \tag{1}$$

where p_μ is the muon momentum and θ^{rel} is the angle between the muon momentum and the direction of the associated jet. Since p_T^{rel} for muons from b-decays is larger than for muons in c-jets, and light-quark or gluon jets (hereafter referred to as light jets), fitting the p_T^{rel} distribution to templates derived separately for b-, c-, and light jets can provide a measurement of the flavor composition of the sample. p_T^{rel} does not depend on a displaced impact parameter or secondary vertex, so it gives an unbiased measure of the efficiencies of those b-taggers that do.

The p_T^{rel} fits are performed both on the b-tagged and non b-tagged samples in order to extract the number of b-quark jets before and after applying the b-tagging requirement. The ratio of these two numbers is an estimate of the semileptonic b-tagging efficiency. The p_T^{rel} method can only measure the b-tagging efficiency in data for semileptonically decaying b-jets. The efficiency scale factor is therefore derived as the ratio between the semileptonic b-tagging efficiency in data and simulation, but is assumed to be identical for hadronically decaying b-jets. The scale factor is measured separately in different bins of the transverse momentum of the b-jet, p_T^{b-jet}.

The p_T^{rel} calibration is now a mature analysis. Although we continue to collaborate on this analysis, the University of Dortmund has taken the lead role in running the calibration on the 2011/2012 data, and we concentrate instead on the *system8* analysis described below.

12.1.2 Calibration of *b*-tagging: the *system8* method.

In this section we describe a procedure for measuring the b-tagging efficiency called *system8*, a data-driven analysis using two samples with different heavy flavor composition and a soft muon tagger in conjunction with the lifetime-based tagger whose efficiency is to be measured. The method, developed within the D0 experiment[70] is more challenging than the p_T^{rel} calibration but ultimately more precise. The Pittsburgh group has developed all the algorithms to compute *system8* inputs from data and from Monte Carlo, implemented a numerical solution to the *system8* equations that properly propagates uncertainties from Monte Carlo inputs, and integrated a semi-analytical solution provided by Grenoble physicists for comparison. Boudreau wrote the core calibration software,

and the *system8* effort has been a collaboration between investigators at NIKHEF, University of Washington, CPPM, Grenoble, and the University of Pittsburgh. The lead graduate student in the early effort on 2010 data was Nancy Tannoury from CPPM in Marseille. Further refinement of the analysis using the 2011 data, including extending the analysis to higher p_T, was done by Mueller and Sapp from Pittsburgh. Mueller also worked with the Dortmund group to coordinate *system8* with p_T^{rel}, so that these analyses could be combined, both with each other and with other measures of b-tagging efficiencies, such as from b-jets in top events.

The *system8* algorithm is a means of constraining eight quantities related to jet tagging rates from observable quantities measured in high-p_T dijet events. It relies on having two samples with different b-fractions, and applying two tagging algorithms to each sample in order to form 8 equations with 8 unknown quantities, among them, the efficiency of the lifetime (LT) b-tagger being calibrated. The first sample, called the n-sample, is the full sample of jets containing at least one muon, and the second one, called the p-sample, a subset of the first one, is formed by requiring one opposite side b-tagged jet. Ideally, the two tagging algorithms must be uncorrelated, therefore in this study, to measure the lifetime b-tagging efficiency, we use an independent tagger which separates b-jets versus c- and light jets using the p_T^{rel} of a soft muon tagger (MT)

The 8 unknowns of the system are the two flavor composition of the two samples (n_b,n_{cl},p_b,p_{cl}) and the two efficiencies for each of the two tagging algorithms (ϵ_b^{LT}, ϵ_{cl}^{LT}, ϵ_b^{MT} , ϵ_{cl}^{MT}); these 8 quantities can be related by 8 equations to 8 observable quantities that also involve coefficients the α_i's, extracted from QCD Monte Carlo (MC), that measure the violation of the assumptions that the tagging efficiency of each tagger is the same on both samples and that the two tagging algorithms are uncorrelated.

These equations constitute a data model which predicts the population within each of the eight subsets. The model is then adjusted to the data, yielding a measurement for all eight of the adjustable parameters, including most prominently the efficiency of the lifetime tagger, ϵ_b^{LT}. The *system8* method is described more fully in [71].

First results from *system8* as run on the 2010 were released as a conference note[56]. The main source of systematic uncertainty in this calibration is the statistical uncertainty of the correlation factors. This is due to limited Monte-Carlo samples. We used the results form the 2010 data to successfully argue for larger Monte-Carlo samples. Updated results using 2011 data were released in spring 2012[57].

Fig. 18 shows the results for the calibration for the MV1 tagger. Most ATLAS physics analyses apply b-tagging directly also to simulated jets. In such context, data/MC scale factors need to be applied to simulated results. These scale factors are also shown in Fig. 18, together with a comparison to the calibration using p_T^{rel}.

12.2 The Measurement of the *b*-jet cross section.

Like the top quark cross section, the b-jet cross section is an important milestone in the program of SM rediscovery. The first two results on b-jet cross sections from ATLAS[58, 59] were for conferences last spring. One of these[59] is the result of one year's collaborative effort between University of Pittsburgh, CPPM, The University of Mainz and the University of Genoa. Boudreau, Mueller and Sapp each contributed to this analysis. When the lead graduate student, Johanna Fleckner of Mainz, finished her Ph.D. and left the field, Mueller assumed the lead role in finishing the analysis. He then worked with the authors of the other conference note, to merge the two analyses into a common publication. The paper based on these results was published at the end of 2011[60].

To perform the analysis, we use a sample of jets containing an associated muon with transverse momentum, $p_T > 4$ GeV. As was explained in the section on Calibration of b-tagging, the

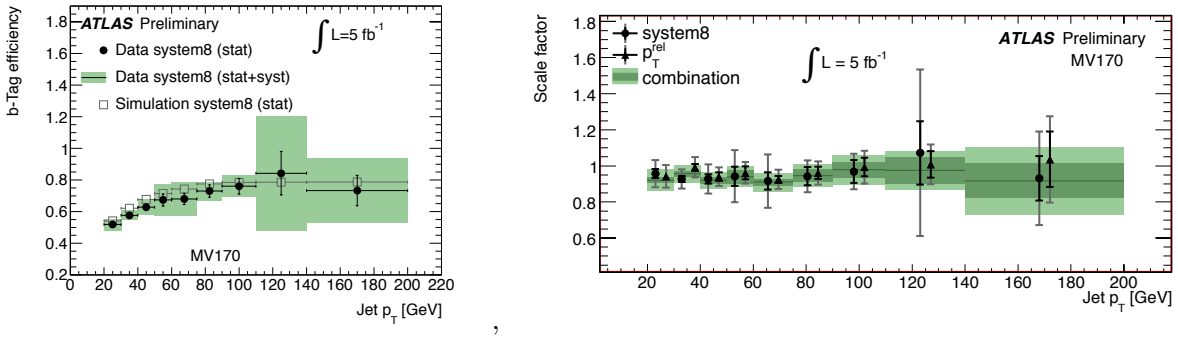

Figure 18: Plots showing the *system8* calibration of the MV1 tagger running at its nominal 70% efficient point. The plot on the left shows b tagging efficiency extracted from *system8* and compared with results from the p_T^{rel} analysis. The plot on the right shows the extracted data-to-Monte-Carlo scale factors for *system8*, p_T^{rel}, and the combination of the two.

distribution of p_T^{rel} has different shapes for c-jets, b-jets, and light jets. The sample composition of jets with associated muons governs the shape of the p_T^{rel} distribution. Fitting the different p_T^{rel} templates for b-, c- and light jets to the p_T^{rel} distribution of jets with associated muons from data provide an estimate of the sample composition, in particular the fraction of b-jets. The b-purity of the sample is measured within four bins of b-jet transverse momentum, p_T^{b-jet}, over a range from 30 GeV through 140 GeV. The results from the fit in the bin $75 < p_T^{b-jet} < 105$ GeV are shown in Fig. 19.

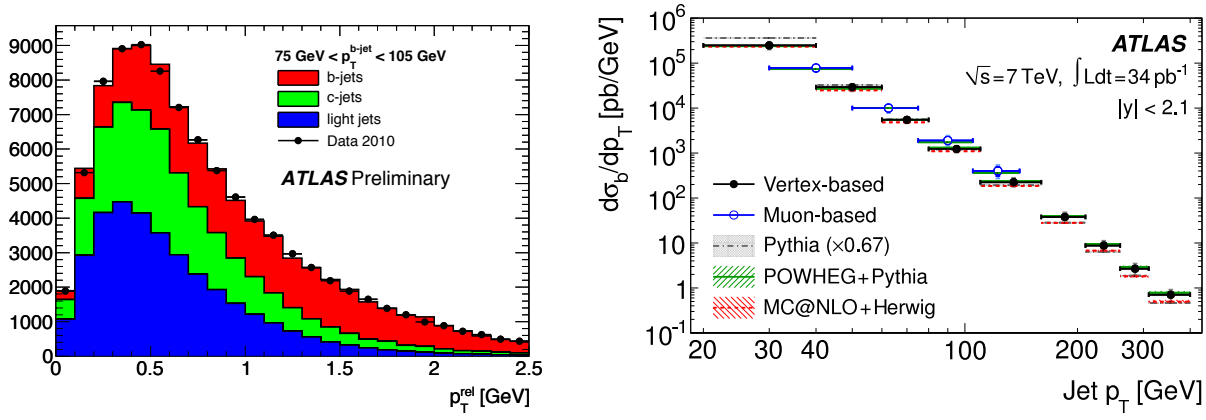

Figure 19: Left plot: p_T^{rel} fit to data in the considered p_T^{b-jet}-bins using the track-based templates. Right plot: Two ATLAS measurements of the b-jet differential cross section $d\sigma(b\text{-}jet, |y^{\mathrm{b-Jet}}| < 2.1)/dp_{\mathrm{T}}^{\mathrm{b-Jet}}$ using the p_T^{rel} of muons in jets (blue) and a reconstructed secondary vertex, SV, (black). Neither statistical correlations nor correlations between the systematic errors of the two measurements such as the luminosity or the jet energy scale uncertainty have been taken into account. The data measurements are compared to two NLO predictions; one using Powheg and Pythia and the other using MC@NLO and Herwig.

Combining the sample purity with the observed event counts, the trigger and reconstruction efficiencies, and the luminosities, we obtain the b-jet production differential cross section. The result is shown in Fig. 19, along with the result from the other analysis[58], which uses information from

the secondary vertex, SV, tagger. In the same figure we compare our measured cross sections to two NLO QCD cross sections predictions. One is computed using the Powheg generator [61] interfaced as in Refs. [62] and [63]. The other is the MC@NLO[64] computation as interfaced to Herwig[65]. As can be seen, there is good agreement between the two measuremenst. The measurements are also in good agreement with the POWHEG prediction. The MC@NLO prediction, at high jet p_T, differs from both the POWHEG prediction and the experimental results. This difference is more pronounced in the central rapidity region. It is an open theoretical question as to the exact source of the difference between these two calculations.

12.3 Measurement anomalous couplings in single top t-channel events

Top quarks are produced in large numbers at the LHC and the data samples currently studied there permit new levels of precision in the measurement of top quark properties. The Pittsburgh group looks for anomalous tensor and pseudotensor couplings of the top quark to the charged weak current, which is important for two reasons. First, since this type of coupling can contribute to CP violation, it sheds light on one of the biggest mysteries in physics today, namely the matter-antimatter asymmetry of the universe. Second, such couplings could also exist in the lighter quarks without being visible, since their effects are suppressed by factors of order M_q/M_W where M_q is the quark mass and M_W is the mass of the W boson.

In the standard model the Wtb vertex is described by the coupling

$$\frac{g}{\sqrt{2}}\bar{b}\gamma^\mu\frac{1}{2}\left(1-\gamma^5\right)tW_\mu^-.$$

However, heavy particles, above the electroweak scale, coupling to the top quark can contribute through radiative corrections to this vertex. The effect such corrections may be absorbed into a small number of so-called anomalous couplings which in an effective field theory can be written as

$$\frac{g}{\sqrt{2}}\bar{b}\gamma^\mu\left(V_LP_L+V_RP_R\right)tW_\mu^- + \frac{g}{\sqrt{2}}\bar{b}\frac{i\sigma^{\mu\nu}}{M_W}q\left(g_LP_L+g_RP_R\right)tW_\mu^-.$$

In this expression, $P_L \equiv \frac{1}{2}(1-\gamma^5)$ and $P_R \equiv \frac{1}{2}(1+\gamma^5)$ are the left and right-handed projection operators, V_L, V_R, g_L, and g_R are complex coupling constants which all (except for V_L) vanish in the standard model, and q is the W boson momentum in the t rest frame. The coupling constant g_R is particularly interesting because a nonzero phase in this coupling would be a new source of CP violation.

The couplings influence the angular distribution of the decay products of polarized top quarks. We select single top quark events produced in the t-channel, Fig. 20 (top left), because in this channel the top quark is highly polarized along the direction of the spectator jet. The angular distribution is described with reference to the direction of the W boson momentum in the top quark frame $\vec{q}$ called the "star" (*) direction, and that of the spectator quark $\vec{s}_t$. These directions are shown in Fig. 20 (top right). Two other directions are then obtained:

$$\begin{aligned}\vec{N} &= \vec{s}_t\times\vec{q}\\ \vec{T} &= \vec{q}\times\vec{N},\end{aligned}$$

The kinematic variables in our analysis are the polar angle θ^* and the azimuthal angle ϕ of the lepton in a coordinate system defined by the vectors $\hat{x}\equiv-\vec{T}$, $\hat{y}\equiv\hat{N}$, and $\hat{z}\equiv\hat{*}$ and shown in Fig. 20 (bottom,right). The analysis is carried out in a simple way by analyzing the projection of the lepton direction onto the $\hat{N}$ direction, and in a more refined way by analyzing the full angular

distribution in (θ^*, ϕ) space. We are taking both approaches, but we consider the first to be merely the tip of the iceberg.

The asymmetry study the distribution of the kinematic variables θ^T and θ^N, defined as the angle between the charged lepton and the vectors $\vec{T}$ and $\vec{N}$, respectively. Expected distributions for fully polarized top quarks are shown in Fig. 21.

These distributions are then described in terms of nine polarization fractions F_i^j where $i \in \{+, -, 0\}$ and $j \in \{*, N, T\}$:

$$\frac{1}{\Gamma}\frac{d\Gamma}{d\cos\theta^*} = \frac{3}{8}(1+\cos\theta^*)F_+^* + \frac{3}{8}(1-\cos\theta^*)F_-^* + \frac{3}{4}\sin^2\theta^* F_0^* \quad (2)$$

$$\frac{1}{\Gamma}\frac{d\Gamma}{d\cos\theta^N} = \frac{3}{8}(1+\cos\theta^N)F_+^N + \frac{3}{8}(1-\cos\theta^N)F_-^N + \frac{3}{4}\sin^2\theta^N F_0^N \quad (3)$$

$$\frac{1}{\Gamma}\frac{d\Gamma}{d\cos\theta^T} = \frac{3}{8}(1+\cos\theta^T)F_+^T + \frac{3}{8}(1-\cos\theta^T)F_-^T + \frac{3}{4}\sin^2\theta^T F_0^T. \quad (4)$$

$$(5)$$

The nine polarization fractions depend on the top couplings V_L, V_R, g_L and g_R (see Ref. [66]). The most interesting experimental observable is the asymmetry (A_{FB}^N) in the normal direction, indicative of a normal W polarization, which has been found to be very sensitive to complex phase g_R in one of the Wtb anomalous couplings:

$$A_{FB}^N \equiv \frac{N(\cos\theta^N > 0) - N(\cos\theta^N < 0)}{N(\cos\theta^N > 0) + N(\cos\theta^N < 0)} = 0.64P\mathrm{Im}(g_R).$$

Any nonzero value for this observable, independent of the polarization, is a sign of a complex Wtb vertex and thus of BSM CP violation in top decays.

The second technique is a full unbinned maximum likelihood fit to the angular distributions of the lepton in the W rest frame. The standard model probability density is shown in an elliptical projection in Fig. 20 (right). This density can be described in terms of three amplitude fractions, three phases, and a polarization, and an unbinned maximum likelihood fit can extract $\mathrm{Im}(g_R)$ independently of the unknown polarization, while using full information about the lepton direction.

The separation of single top events from a background of QCD multijets and W+heavy flavor and $t\bar{t}$ backgrounds is already a major exploit. The sample of single top t-channel candidate events has a large background contamination and is highly sculpted by cuts. In addition, effects such as neutrino momentum reconstruction smear the reconstruction of the directions that define the coordinate system and therefore also the kinematic variables. We have found an innovative way to incorporate these effects analytically into the double differential cross section. The technique is used then to construct an analytic, normalized, smeared, efficiency-corrected fitting function that includes backgrounds. The function intrinsically describes the joint $\cos\theta^*$ and ϕ distribution. In Fig. 22 we have projected the function onto the $\cos\theta^*$ and ϕ axes (red; the background contribution alone is shown in blue). This is co-displayed with simulated data from toy Monte Carlo which is *almost completely obscured by the fitting function.* To construct the fitting function, first one characterizes the efficiency, background, and directional resolution of the detector; this information is then combined with the underlying physics distrubution to construct the fitting function, which can be adjusted to data through five adjustable parameters including three amplitude fractions, two phases, and the polarization. Constraints on all of these can be obained from a fit to the parameters. The techniques are similar to those employed in the $J/\psi\phi$ analysis, Section 3.2, and the anticipated results will be presented in a similar way.

This study of single top t-channel events depends on dedicated single top ntuples, background estimates, and Monte Carlo samples. The single top group in ATLAS is a partnership and some

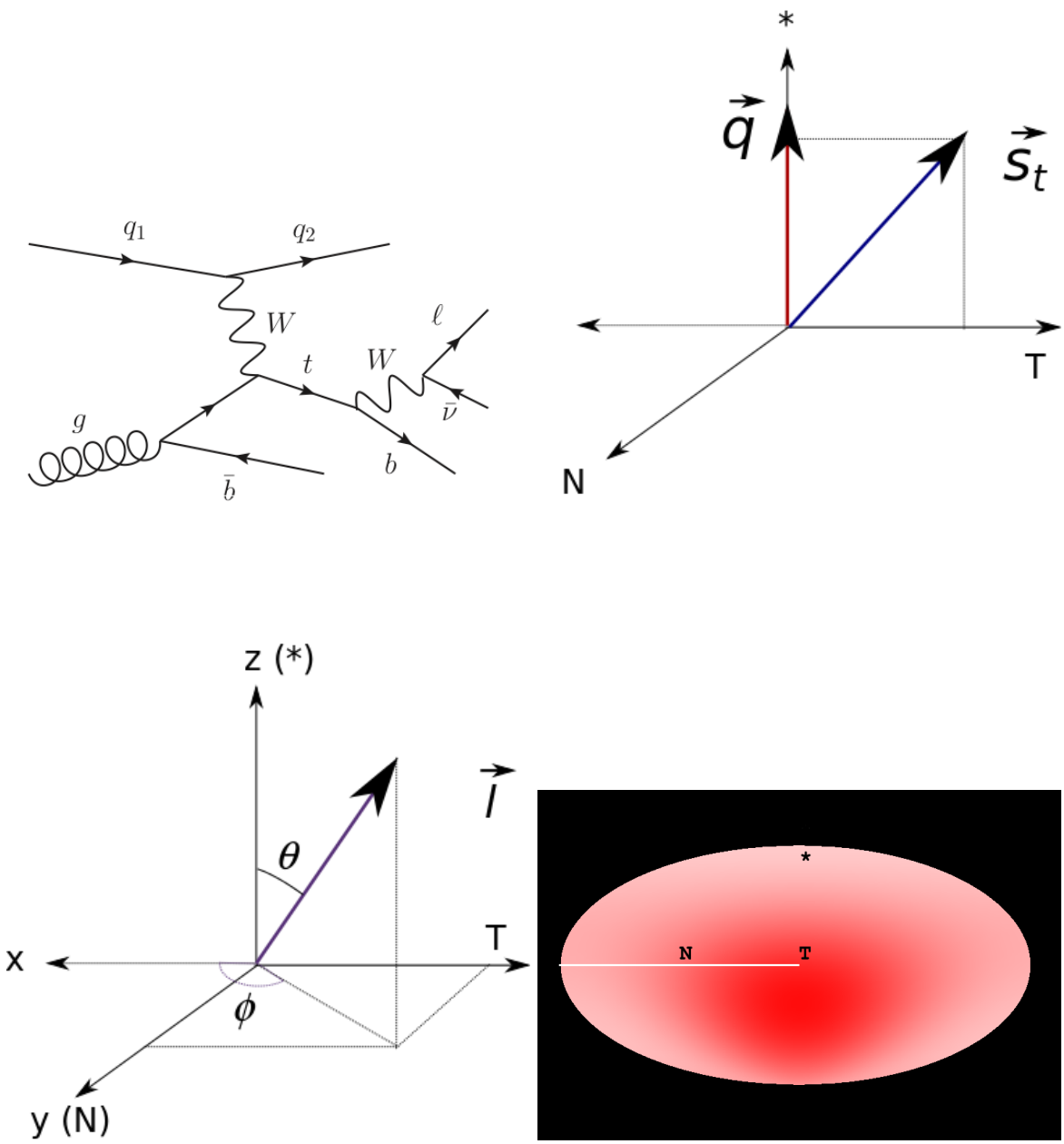

Figure 20: Top row: Feynman diagram for the t-channel production of single top (right); the definition of the $\hat{T}$ and $\hat{N}$ direction (left). Bottom row: definitions of polar and azimuthal angles used in the description of the lepton direction (left); an elliptical projection of the joint probability density $\rho(\cos\theta, \phi)$ (right).

of these tasks are carried out by our colleagues from other institutes. We have been mostly active in setting up the production of the PROTOS[68] event generator to simulate single top production including anomalous couplings. This event generator was recently interfaced to the ATLAS simulation by Escobar, and compared against the standard event generator used for single top production, AcerMC. We are also involved in the ntuple production for the analysis, which is useful for our groups as well as other groups studying t-channel single top. Both analysis described in this section are already interesting using 2011 data, and the analysis is ongoing. Pittsburgh is the leader of

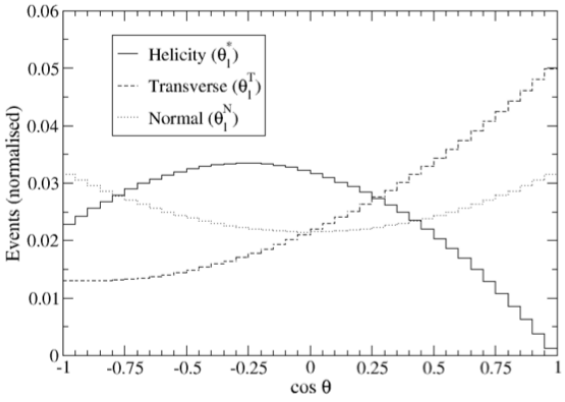

Figure 21: Expected distributions of θ^*, θ^N, and θ^T for standard model values of top quark couplings. These are "bare" distributions and need to be diluted for partially polarized top events. The plots are from Ref. [66].

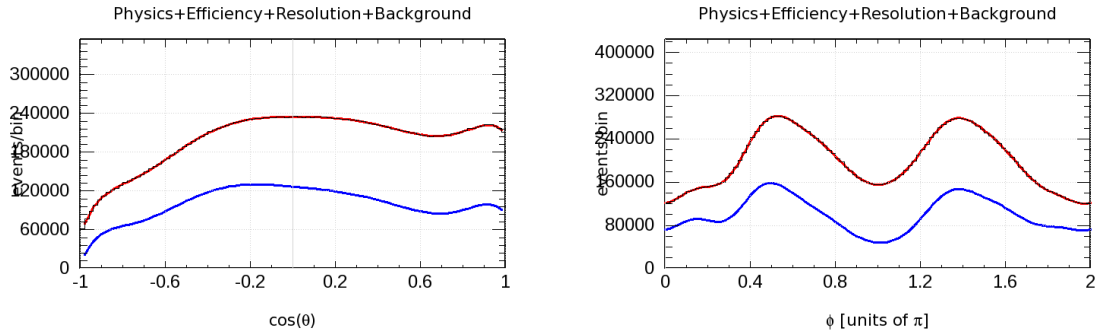

Figure 22: Plot showing the fitting function used to extract physical observables from the angular distributions of polarized single top quarks. The distributions are obtained from an arbitrary point in the parameter space. The red curve shows the analytic fitting function; it sits directly on top of simplifed Monte Carlo events which are obscured by the curve. The blue curve shows the background shape.

the analytic fitting method and also participates fully in the asymmetry measurement. In 2012 the statistics will already increase more than fourfold and we will then repeat the analysis for a definitive measurement. It is anticipated that Sapp will earn his Ph.D on the 2011 data while Su will earn a Ph.D on 2012 data.

References

[1] G. Aad *et al.* [ATLAS Coll.], Eur. Phys. J. C **72**, 2056 (2012) [arXiv:1203.5420 [hep-ex]].
[2] G. Aad *et al.* [ATLAS Coll.], JINST **3** (2008) S08003.
[3] G. Aad *et al.* [ATLAS Coll.], JHEP **12** (2010) 060.
[4] M. Cacciari and G. P. Salam Phys. Lett. **B641** (2006) 57.
[5] M. Cacciari, G. P. Salam and G. Soyez, `http://fastjet.fr/`.
[6] E. Abat *et al.*, [ATLAS Coll.], Nucl. Instr. Meth. A621 (2010) 134.
[7] G. Aad *et al.* [ATLAS Coll.], Tech. Rep. ATLAS-CONF-2010-099, 2010.
[8] B. Aharmim *et al.* [SNO collaboration], Phys. Rev. **C 72** (2005) 055502.
[9] A. Davidson, K. C. Wali, Phys. Rev. Lett. **60** (1987) 18.
[10] F. Aguila, S. Bar-Shalom, A. Soni, J. Wudka, Phys. Lett. **B 670** (2009) 399–402.
[11] R. N. Mohapatra and J. C. Pati, Phys. Rev. D **11**, 2558 (1975).
[12] R. N. Mohapatra, ISBN 0-387-95534-8, Springer-Verlag, 3rd ed., 2002.

[13] R. N. Mohapatra and P. B. Pal, ISBN 981-238-070-1. World Scientific, 3rd ed., 2004.
[14] The L3 Coll., Phys. Lett. **B517**:67-74 (2001).
[15] The L3 Coll., Phys. Lett. **B295**:371-382,1992 (1992).
[16] S. Abachi *et al.* [D**0** Coll.], Phys. Rev. Lett. **76**, 3271-3276 (1996);
[17] V. M. Abazov *et al.* [D**0** Coll.], Phys. Rev. Lett. **100**, 211803 (2008).
[18] G. J. Feldman and R. D. Cousins, Phys. Rev. D **57**, 3873-3889 (1998).
[19] A. Abulencia *et al.* [CDF Coll.], Phys. Rev. Lett. **98**, 221803 (2007); D. E. Acosta *et al.* [CDF Coll.], Phys. Rev. Lett. **93**, 061802 (2004).
[20] CMS Coll., CERN-PH-EP-2011-009, arXiv:1102.4746 [hep-ex].
[21] T. Aaltonen *et al.* [CDF Coll.], Phys. Rev. Lett. **104**, 091801 (2010).
[22] T. Aaltonen *et al.* [CDF Coll.], Phys. Rev. Lett. **102**, 041801 (2009); A. A. Affolder *et al.* [CDF Coll.], Phys. Rev. Lett. **87**, 251803 (2001); F. Abe *et al.* [CDF Coll.], Phys. Rev. Lett. **83**, 2133-2138 (1999).
[23] V. M. Abazov *et al.* [D**0** Coll.], Phys. Rev. Lett. **97**, 151804 (2006).
[24] B. Schremp and F.Schremp, Phys. Lett. **153B** (1985) 101.
[25] H. Georgi and S. Glashow, Phys. Rev. Lett. **32** (1974) 438.
[26] J. Pati and A. Salam, Phys. Rev. **D10** (1974) 275.
[27] G.Senjanovic and A.Sokorac, Z. Phys. **C20** (1983) 255.
[28] P. Frampton and B.-H. Lee, Phys. Rev. Lett. **64** (1990) 619.
[29] P. Frampton and T. Kephart, Phys. Rev. **D42** (1990) 3892.
[30] E. Witten, Nucl. Phys. **B258** (1985) 75.
[31] M. Dine *et. al.*, Nucl. Phys. **B259** (1985) 519.
[32] K. Lane, Nucl. Phys. (1993) , `hep-ph/9401324`.
[33] O. Shanker, Nucl. Phys. **B204** (1982) 375.
[34] W. Buchmuller and D.Wyler, Phys. Lett. **B177** (1986) 377.
[35] M. Kramer *et al.*, Phys. Rev. **D71** (2005) 57503.
[36] L. Hewett and T. G. Rizzo, Nucl. Instrum. Meth. **A434** (1999) 435–443.
[37] P. Langacker, Rev. Mod. Phys. **81** (2009) 1199–1228.
[38] J. Erler, P. Langacker, S. Munir, and E. R. Pena, JHEP **0908** (2009) 017.
[39] M. Chizhov, V. Bednyakov, and J. Budagov, Phys. of Atom. Nucl. **71** (2008) 2096–2100.
[40] L. Randall and R. Sundrum, Phys. Rev. Lett. **83** (1999) 3370–3373.
[41] K. D. Lane and E. Eichten, Phys. Lett. **B222** (1989) 274.
[42] D. London and J. L. Rosner, Phys. Rev. **D34** (1986) 1530.
[43] M. Dittmar, A.-S. Nicollerat, and A. Djouadi, Phys. Lett. **B583** (2004) 111–120.
[44] M. Chizhov and G. Dvali, `arXiv:0908.0924 [hep-ph]`.
[45] M. V. Chizhov, Phys. of Part. and Nucl. Lett. **8** (2011) 6.
[46] M. V. Chizhov, V. A. Bednyakov, and J. A. Budagov, Nuovo Cimento **C33** (2010) 343.
[47] C. Hays, A. V. Kotwal, and O. Stelzer-Chilton, Mod. Phys. Lett. A **24** (2009) 2387; and references therein.
[48] G. Abbiendi *et al.* [OPAL Coll.], Eur.Phys.J. **C33** (2004) 173–212.
[49] J. Abdallah *et al.* [DELPHI Coll.], Eur. Phys. J. **C45** (2006) 589–632.
[50] P. Achard *et al.* [L3 Coll.], Eur.Phys.J. **C47** (2006) 1–19.
[51] S. Schael *et al.* [ALEPH Coll.], Eur. Phys. J. **C49** (2007) 411–437.
[52] V. M. Abazov *et al.* [D0 Coll.], Phys. Lett. **B695** (2011) 88–94.
[53] T. Aaltonen *et al.* [CDF Coll.], Phys.Rev.Lett. **106** (2011) 121801.
[54] CMS Coll., `arXiv:1103.0981 [hep-ex]`.
[55] A. Caldwell, D. Kollar, and K. Kröninger, *BAT - The Bayesian Analysis Toolkit*, Comp. Phys. Comm. **180** (2009) 2197.
[56] ATLAS Coll., ATLAS-CONF-2011-143 (2011).
[57] ATLAS Coll., ATLAS-CONF-2012-043 (2012).
[58] ATLAS Coll., ATLAS-CONF-2011-056 (2011).
[59] ATLAS Coll., ATLAS-CONF-2011-057 (2011).

[60] ATLAS Coll., EPJ **C71** (2011).
[61] Alioli,S. and Hamilton,K. and Nason,P. and Oleari,C. and Re,E., JHEP **06** (2010) 43.
[62] Stefano Frixione, *et al.*, JHEP **11** (2007) 70.
[63] R. Corke and T. Sjöstrand, arXiv:1003.2384v1 [hep-ph].
[64] S. Frixione and B. R. Webber, JHEP 06 (2002) 029, JHEP 08 (2003) 007.
[65] G. Corcella et al., JHEP 01 (2001) 010.
[66] J. A. Aguilar-Saavedra and J. Bernabeu, Nucl. Phys. **B840** (2010) 349.
[67] ATLAS Coll., ATLAS-CONF-2011-037 (2011).
[68] J. A. Aguilar-Saavedra *et al.*, Eur. Phys. J. **C50**) (2007) 519.
[69] ATLAS Coll, ATLAS-CONF-2011-035 (2011)
[70] V.M. Abazov et al., b-Jet Identification in the D0 Experiment, Nucl. Instrum. Meth. A620 (2010) 490-517
[71] G. Aad et al. [The ATLAS Collaboration], Expected Performance of the ATLAS Experiment –Detector, Trigger and Physics, CERN-OPEN-2008-020, arXiv:0901.0512 [hep-ex], 2009.1
[72] R. Kleiss and W.J. Stirling, Z. Phys. C **40** 419-423 (1988)